Propagation of cosmic rays in the Earth's atmosphere

A. Putze

Master Thesis

Master 2 of Physics and Engineering: Subatomic Physics and Astroparticles

Joseph Fourier University at Grenoble

Propagation of cosmic rays in the Earth's atmosphere

Antje Putze

Internship at the LPSC Grenoble
Supervised by Laurent Derome

June 2006

Acknowledgements

First of all I want to thank Michel Buénerd, teamleader of the AMS/CREAM group of the LPSC Grenoble, for hosting me the second year in his team and for his infectious enthusiasms.

The biggest thanks goes to Laurent Derome, who affiliates me as an apprentice. I respect him not only for his merits in Physics but also for his patience in enduring and answering even my stupidest questions, resolving my progamming problems in between minutes, going through the thesis text a dozen of times and accepting me in his office.

I want to thank David Maurin for making this thesis work possible in that short time, for giving support even online from Dublin, Turin, Lisbon or other foreign places and for being such a kind email contact.

What would I be without my friends? Yoann, you are the greatest! Thanks for your help in all questions concerning ROOT, C++, ..., as well as for the thousands of taxi tours with your beloved AX. Thanks to you Stéph for supporting me morally during the last university year and for your unlimited help. Thanks too to Björn, my discussion partner for physical, informatical and private items and my chocolate-break partner, another German in the LPSC, who also supported me in my studies. To Christian, who left the LPSC and left us alone. Preparing and making presentations with you did belong to the best moments during the Master 2 course. Last but not least I would like to thank all the PhD-students for the most beautiful parties, BBQ's, football matches, and so on.

Résumé

Le rayonnement cosmique est composé de particules chargées, qui arrivent après un long trajet à travers la galaxie sur la Terre. Les explosions de supernova sont supposées être les sources galactiques, qui accélèrent ce rayonnement jusqu'aux énergies d'environ 10^{18} eV. Au-delà de cette énergie, on suppose que des sources extragalactiques, comme par exemple des noyaux actifs de galaxie (AGN), des gamma ray bursts ou des pulsars sont à l'origine du rayonnement cosmique d'ultra hautes énergies. L'indice spectral des distributions en énergie des éléments du rayonnement cosmique reflète la dynamique de sa propagation, en particulier la conjugaison des effets liés au spectre de source du rayonnement cosmique et ceux liés à sa propagation (accélération, absorption et échappement). L'évolution de l'indice spectral avec l'énergie des particules du rayonnement cosmique constitue un test sensible des composantes qui déterminent cette évolution. La mesure précise des indices des spectres individuels des éléments du rayonnement cosmique par AMS jusqu'au TeV et par l'expérience CREAM au-delà, du TeV au PeV, vont clairement permettre d'avancer dans cette problématique. Une des difficultés de cette mesure est de bien prendre en compte les erreurs systématiques. En particulier, il faut lors de l'analyse des données prendre en compte l'interaction (diffusion et fragmentation) des ions pendant leur traversée dans l'atmosphère. L'étude de l'interaction et de la fragmentation des ions dans l'atmosphère est donc indispensable et décrite dans ce travail. L'étude se base sur un calcul matriciel, qui a été implémenté et testé avec succès et qui a permis d'analyser les effets, causés par des incertitudes expérimentales sur les sections efficaces, sur la mesure de l'indice spectral.

Abstract

Cosmic rays are composed of charged particles, which arrive after a long travel through the Galaxy on Earth. Supernova explosions are considered to be galactic sources, which accelerate these particles up to energies around 10^{18} eV. Beyond this energy, one supposes that the extragalactic sources, like active galaxy nuclei (AGN), gamma ray bursts or pulsars, are the origin of the ultra high energy cosmic rays. The spectral index of the elemental energy distributions of cosmic rays reflects the dynamic of its propagation, particularly the conjugation of the effects connected to the cosmic ray source spectrum and those connected to its propagation (acceleration, absorbtion and escape). The evolution of the spectral index with the cosmic-ray particle energy constitutes a sensitive test of the components, which determine this evolution. The precise index measurement of individual elemental spectra of the cosmic rays by AMS up to TeV and by the experiment CREAM beyond it, from TeV to PeV, will permit to proceed in this problematic. One of the difficulties on this measurement is to take well into account the systematic errors. During the data analysis we have to take into account in particular the interaction (diffusion and fragmentation) of the ions while their travel through the Earth's atmosphere. The study of the interaction and the fragmentation of these ions in the atmosphere is hence indispensable and described in this work. The study is based on a matrix calculation, which had been successfully implemented and tested and which has permitted to analyse the effects, caused by the experimental uncertainties on the cross sections, on the spectral index measurement.

Contents

Introduction **1**

1 Cosmic Rays **2**
1.1 A little bit of history... 2
1.2 Some general properties 3
1.2.1 Energy spectrum 3
1.2.2 Composition and abundances 4
1.2.3 Origin and acceleration 4
1.3 Propagation 5
1.3.1 Basic diffusion equation 5
1.3.2 Galactic wind 5
1.3.3 Reacceleration 5
1.3.4 Full diffusion equation 6
1.3.5 Some custom models 6
1.4 Solar Modulation and fluxes on the top of the atmosphere 8
1.4.1 Force field solar modulation 8
1.4.2 Top of the atmosphere (TOA) and interstellar (IS) fluxes 9
1.5 Physics of cosmic rays 9
1.5.1 Dark matter 9
1.5.2 Constraints on the propagation parameters 10
1.6 Detection of cosmic rays 12
1.6.1 Direct detection 12
1.6.2 Experiments 13
1.6.3 Indirect detection 14
1.6.4 Experiments 15

2 Propagation of cosmic rays in the Earth's atmosphere **17**
2.1 Structure and composition of the Earth's atmosphere 17
2.2 Fragmentation process 18
2.3 Transport equation 19

3 Cross sections **20**
3.1 Total inelastic cross sections 20
3.1.1 The empirical Webber formula 20
3.1.2 The semi-empirical formula by Letaw & al 20
3.1.3 Universal parametrisation of Tripathi & al 21
3.2 Fragmentation cross sections 22
3.2.1 Semi-empirical formula by Silberberg and Tsao 22
3.2.2 Empirical formula by Webber & al 23
3.2.3 Factorisation 24
3.3 Implementation with the USINE software 24

4 Study of the fragmentation process in the Earth's atmosphere **27**
4.1 Implementation of the transport equation 27
4.2 Unfolding test 29
4.3 Error study 30
4.4 Results 32

5 Conclusions **34**

Introduction

The study of cosmic rays originated approximately in 1900, as a result of the observation of the ionisation in gases contained in closed vessels. To elucidate the role of the Earth balloon flights were undertaken. They led to the definite discovery of cosmic rays by V. Hess in 1912. By 1950 the main features of the composition of primary cosmic rays were known. But the very detailed information available on the composition and the energy spectrum of the cosmic rays on Earth says little about their sources and especially about the location of these sources. So one of the central questions of the astrophysics of cosmic rays is the problem of their origin.

The details of the specific physical mechanism, where a decisive role is played by the galactic magnetic field, that regulates the motion of cosmic rays are yet not known. Because of the absence of a definite theory that explains the nature of the propagation of cosmic rays based on a rigourous picture of the interaction of charged relativistic particles with the interstellar medium, one uses approximate semi-empirical models.

The evolution of the spectral index, which is one essential parameter of the propagation models, with the cosmic ray particle energy constitutes a sensitive test of the components, which determine this evolution. The precise index measurement of individual elemental spectra of the cosmic rays by AMS up to TeV and by the experiment CREAM beyond it, from TeV to PeV, has some difficulties, where one of these is to take well into account the systematic errors. In particular, we have during the data analysis, to take into account the interaction (diffusion and fragmentation) of the ions while they travel through the Earth's atmosphere or through the detector.

The first chapter of this work is entirely dedicated to cosmic rays. We will begin with a small introduction of the cosmic-ray history and then pass to the description of the cosmic-ray properties, i.e. the energy spectrum, the composition, and abundances of the cosmic ray fluxes and finally, the theoretical approaches for the origin and acceleration. Once we know were the cosmic rays are supposed to be produced and accelerated, we will go into the question of cosmic-ray propagation. We will present here three of the most common propagation models: the diffusion, leaky box and weighted slab model. Then, arrived in the solar system, cosmic rays are modulated by the solar magnetic fields before arriving at the Earth. The cosmic-ray detection can be made directly with the help of space-based or balloon experiments and indirectly with the help of ground-based detectors measuring the secondary particles produced in extensive air showers. We will present these two detection types and give for each type two examples of recent experiments, which aim to elucidate the propagation of cosmic rays in the interstellar medium.

For our study of the cosmic ray propagation in the Earth's atmosphere it is indispensable to know its structure and composition. This will be discussed in the second chapter, where we want to introduce the atmosphere model used for the fragmentation calculation. The fragmentation process of cosmic rays in the Earth's atmosphere will be presented, which permits us to establish the transport equation, which can be used for modelling the propagation of cosmic rays in the atmosphere.

Cross sections are used by the transport equation for the interaction of the cosmic-ray particles in the Earth's atmosphere. In the third chapter we will discuss the two types of cross sections, associated with the absorption of a given nucleus and the production of a given nucleus from a heavier nucleus, and the different existing approaches for the total inelastic and the fragmentation cross section calculation. In this work the used fragmentation cross section parametrisation is based on nucleus-hydrogen and nucleus-helium reactions. Therefore a scaling factor is used for calculating the fragmentation cross sections for nucleus-nucleus reactions, which is done with the help of the USINE software.

The study of the fragmentation process in the Earth's atmosphere is entirely described in chapter 4. At first the implementation methods are represented (iterative integration and matrix calculation). The latter will be tested for unfolding problems, which could be caused by statistical fluctuations. Then, the systematical error on the data reconstruction, due to the experimental uncertainties on the cross sections, will be estimated. At last we will discuss the results obtained.

1 Cosmic Rays

1.1 A little bit of history... [1, 2] [3]

At the turn of the 19^{th} century some of the great mysteries of electricity were explored and resolved. The cosmic-ray history begins at this time when it was found out that electroscopes or other electrically charged vessels discharged and gases contained in closed vessels ionised, even if they were kept in the dark well away from sources of natural radioactivity. The origin of this behaviour was a major puzzle and various ingenious experiments were carried out to discover the origin of this ionising radiation.

Theodor Wulf, a German Jesuit priest and physicist, who constructed the most precise electrometers at the time, which was the standard for generations, was interested in the source of the radiation. The current opinion was that the radioactive elements in the Earth cause it. Further, one knew that radioactive radiation is absorbed in the air, hence the intensity decreases with the distance of its sources. Theodor Wulf concluded that the radiation intensity must decrease with growing distance from Earth. γ-rays were the most penetrating of all the ionising radiation known at that time and their absorption coefficient in air was also known. If the ionisation had been due to γ-rays, originating at the surface of the Earth, the intensity of ions should halve in only 80 m. He found that the ionisation fell from $6 \times 10^6\,\text{ions} \cdot \text{m}^{-3}$ to $3.5 \times 10^6\,\text{ions} \cdot \text{m}^{-3}$ as he ascended the Eiffel Tower in 1910, a height of 330 m, where the intensity of the radiation should have been negligible. He published a paper in *Physikalische Zeitschrift* detailing the results of his four days of observation on the Eiffel Tower. But his results were not initially accepted.

Theodor Wulf hypothesised audaciously that the assumption that the Earth is the source of the radioactivity is false and that it is the cosmos from where the extraterrestrial radiation fall down on the atmosphere. For approving his theory Wulf called on his physicist colleagues to perform measurements in great height with hang gliders and balloons.

The big breakthrough came in 1912 when the Austrian physicist Viktor Hess made manned balloon ascents during which he measured the ionisation. Especially successful was his flight on 7 August 1912, when he reached an altitude of 5 km. At this altitude the ionisation rate was several times that observed at sea level. These results were confirmed in 1913-1914 by the German physicist Werner Kolhörster, who reached altitudes of 9 km, where the ionisation rate was even higher. This was a clear evidence that the source of the ionising radiation must be located above the Earth's atmosphere. From the observed decrease in the number of ions $n(l)$ at a distance l through the atmosphere, the attenuation constant α, defined by $n(l) = n_0 \text{e}^{(-\alpha l)}$ could be found. From the data of Kolhörster it was found that the values of α was equal to $10^{-3}\,\text{m}^{-1}$ or less. This can be compared with the absorption coefficient for the γ-rays from radium C, which in air has a value of $4.5 \times 10^{-3}\,\text{m}^{-1}$, i.e. the γ-rays from radium C are at least five times less penetrating than the ionising radiation which must originate from above the atmosphere.

Figure 1: Viktor Hess

It was not too much of an extrapolation to assume that the *ultra γ-rays*, named so by the discoverer Viktor Hess of the *cosmic radiation* or *cosmic rays*, as they were named by Millikan in 1925, were γ-rays with greater penetrating power than those observed in natural radioactivity.

The year 1929 saw the invention of the *Geiger-Müller detector* which enabled individual cosmic rays to be detected. In the same year, the two German physicists Walter Bothe and Werner Kolhörster performed one of the key experiments in cosmic ray physics. The object of the experiment was to determine whether the cosmic radiation consisted of high energy γ-rays or charged particles. By using two counters, one placed above the other, they found that simultaneous discharges of the two detectors occurred very frequently, even when a strong absorber was placed between the detectors, indicating that charged particles of sufficient penetrating power to pass through both of them were very common. The experiment strongly suggested that the cosmic radiation consists of charged particles. Finally they noted that the particles would have to be very energetic because of their long ranges in matter. They estimated the energies of the particles to be about $10^9 - 10^{10}\,\text{eV}$.

1.2 Some general properties

Since the discovery of cosmic rays, many scientists studied this phenomenon and assembled some characteristic properties of these ionised particles. Starting with the energetic spectrum, which offers us two physical riddles over a great energy range, we will discuss in this section also the composition and abundances of cosmic rays, which could us tell more about its origin. Then, we will introduce some propagation models, of which the aim is to explain the cosmic-ray propagation in the interstellar medium. Arriving in the solar system, the charged particles interfere with the Sun's and the Earth's magnetic fields, which additionally modify the cosmic-ray abundances. The detection of cosmic rays on the Earth's surface and in the Earth's upper atmosphere is a great physical challenge, knowing the great energy range of cosmic rays, but it is also of great physical interest. Predominantly, the secondary-to-primary ratios can tell us a lot about our Galaxy (structure and composition) and about the physical processes which occurs in the Galaxy, like the propagation.

1.2.1 Energy spectrum

The primary cosmic-ray particles extend over at least 13 decades in energy with a corresponding decline in intensity of over 32 decades. The spectrum is remarkably featureless with little deviations from a constant power law

$$\frac{\mathrm{d}N(E)}{\mathrm{d}E} \propto E^{-\gamma}$$

across this large energy range. The flux of cosmic rays falls off rapidly as the cosmic-ray energy increases. Particles with an energy below $10^6\,\mathrm{eV}$ originate from the solar wind. Even until an energy of $10^{10}\,\mathrm{eV}$ the cosmic rays are modulated by solar activity (discussed in section 1.4). The rate of arriving particles with energies $E \geq 10^6\,\mathrm{eV}$ is about 10^4 per square metre per second. For energies above $10^{12}\,\mathrm{eV}$, the rate is only one particle per square metre per second. The rate starts to decrease even more rapidly around $3 \cdot 10^{15}\,\mathrm{eV}$. That small change in slope, from $E^{-2.7}$ to $E^{-3.0}$, is known as the "knee" of the cosmic ray spectrum. At these energies, there are only a few particles per square metre per year. The highest energy particles, above $10^{19}\,\mathrm{eV}$, arrive only at a rate of about one particle per square kilometre per year. The "knee" itself is quite interesting, because we do not yet understand why the spectrum experiences an abrupt change in slope at that point. There is also an "ankle" in the spectrum around $10^{19}\,\mathrm{eV}$, where the rate is found to be somewhat higher than expected. Here the slope changes to a value of -2.8. At this energy one expects a cut-off, a theoretical upper limit of the cosmic rays from distant sources. This limit, called GZK-limit, was computed in 1966 by Kenneth Greisen, Vadim Kuzmin and Georgiy Zatsepin, based on interactions predicted between cosmic rays and photons of the cosmic microwave background radiation. They predicted that cosmic rays with energies over the threshold energy of $5 \cdot 10^{19}\,\mathrm{eV}$ would interact with cosmic microwave background photons to produce pions. This would continue until their energy fell below the pion production threshold. Therefore, extragalactic cosmic rays with energies greater than this threshold energy should never be observed at Earth.

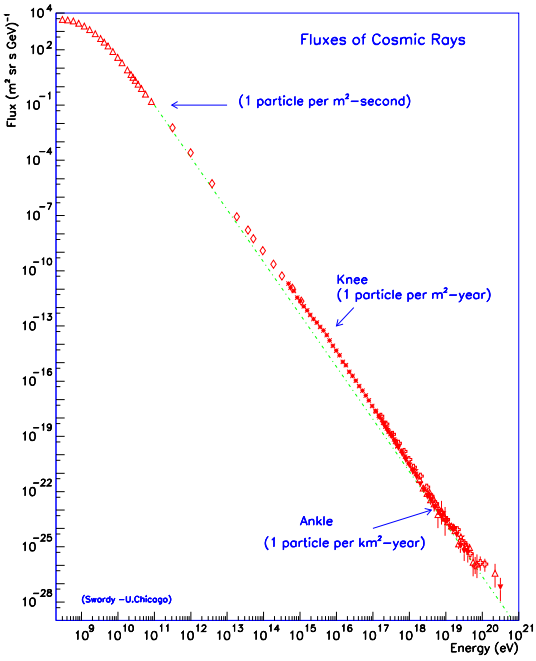

Figure 2: Differential cosmic ray flux [4]

Because of this featureless spectrum, it is believed that cosmic-ray production and propagation is governed by the same mechanism over decades of energy at least below the knee and that the same or another one works above the knee.

1.2.2 Composition and abundances

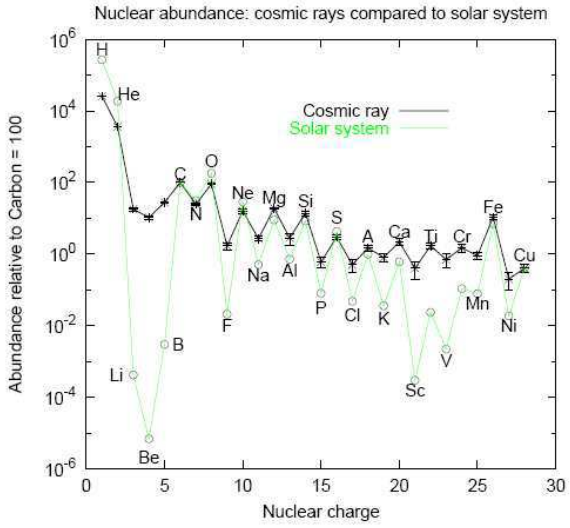

Figure 3: Relative chemical abundances of cosmic rays and of the solar system, normalised to C [5]

Cosmic rays includes the galactic, anomalous cosmic rays and solar energetic particles. The galactic cosmic rays reach us from the solar system and the anomalous cosmic rays from the interstellar space at the edge of the heliopause (boundary where the Sun's solar wind is stopped by the interstellar medium). The solar energetic particles are associated to solar flares and other energetic solar events. The term "cosmic rays" used to include X-rays and γ-rays, but we are only interested in the charged particles with no solar system origin.

The chemical abundances of cosmic rays provides important clues to their origin and to the processes of propagation from their sources to the Earth. The composition of cosmic rays up to an energy of 1 TeV is well known. In terms of numbers about 98% of the particles are nuclei and 2% are electrons. Of the nuclei about 87% are protons, 12% are helium nuclei and the remaining 1% are heavier nuclei. We can see in the figure 3 [5] the relative abundance of the different cosmic-ray elements compared to these of the Solar System. The distribution of element abundances in cosmic rays is not so different from those of typical solar system abundances. Both distributions have peaks at carbon, nitrogen and oxygen and the iron group, which could be explained by the fact that cosmic-ray particles must have been accelerated from material of quite similar chemical composition to the Solar System abundances. On the other hand, there is an excess abundance in cosmic rays for the light elements, lithium, beryllium, and boron, and for elements with atomic mass numbers just less than those of iron, i.e. the elements calcium to manganese called the sub-Fe group. This is the result of spallation of the more abundant primary cosmic ray nuclei, especially carbon and oxygen, as we shall discuss later in section 2.2. Finally, there is an underabundance of hydrogen and helium, probably resulting from their high ionisation potential, which make them less available for the acceleration.

1.2.3 Origin and acceleration

The energy spectrum, the composition, and the abundances of the observed cosmic rays could probably tell us more about their origin and their acceleration in the Universe. In contrary to neutrinos and γ-rays, which point directly to their sources, charged particles are deviated by interstellar magnetic fields. As consequence, the cosmic rays arriving at Earth are practically isotropic. Anisotropy could be an indicator for point-like sources, but this is only expected for energies above 10^{18} eV. The information on the composition of cosmic rays should help identifying the main sources. The candidates for galactic cosmic-ray sources must bring up a high power in the aim to assure an energy density of $1\,\mathrm{eV/cm^3}$, like supernova explosions. However, cosmic rays have been observed at much higher energies than supernova remnants can generate, and where these ultra-high energies come from is a big question. Perhaps they come from outside the Galaxy, from pulsars, neutron stars, binary systems, active galaxy nuclei (AGN) and gamma-ray bursts, which could be considered as high energy (extragalactic) cosmic-ray sources.

One of the most intriguing problems in high energy physics is the mechanisms by which the high energy particles are accelerated to ultrarelativistic energies. Therefore we must consider some specific features for this acceleration. First the acceleration mechanism must reproduce the typical energy spectrum of cosmic rays, which has the form of a power law: $\frac{\mathrm{d}N(E)}{\mathrm{d}E} \propto E^{-\gamma}$. Second it should be able to accelerate the cosmic rays up to energies $E \sim 10^{20}$ eV. At last the acceleration mechanism should reproduce the observed chemical abundances of cosmic rays.

We can divide the acceleration mechanism in three classes: dynamic acceleration which takes place through the collision of particles with clouds, hydrodynamic acceleration, which involves whole layers of plasma to high velocities, and electromagnetic acceleration including the electric field processes, like electromagnetic or plasma waves and the magnetosphere of neutron stars.

The Italian physicist Enrico Fermi proposed in 1949 an acceleration mechanism by which particles colliding with clouds in the interstellar medium could be accelerated to high energies. Charged particles, stochastically diffused, are reflected from irregularities in the Galactic magnetic field, which move randomly with a typical velocity V. The particles gain energy statistically in each reflection proportional to the second order in V/c [2].

This is called the second order Fermi acceleration. This mechanism could not be the main source of energy for the particles, because the energy gain resulting of these collisions is too slow and insignificant. If we consider only head-on collisions the energy increases with the first order in V/c. This is called the first order Fermi acceleration, which is very effective in presence of strong shock waves, like those associated with supernova explosions and which conduct naturally to a differential energy spectrum of the high energy particles with a slope of the order of -2 [2].

1.3 Propagation

The high isotropy of cosmic rays indicates effective mixing and long travel time for high-energy particles in the Galaxy, where the galactic magnetic field plays a decisive role. However, the propagation mechanisms of cosmic rays are as yet not fully known. But considering all the known phenomena in the Galaxy, one can formulate propagation models, which aim to explain the cosmic ray propagation in the Galaxy. Three very common used propagation models will be shortly presented here: the diffusion, the Leaky Box, and the weighted slab model.

1.3.1 Basic diffusion equation

The propagation model considered most frequently is the diffusion model, which is described by the basic transport equation for a particle i with density $N_i(t, \vec{r}, E_k)$ [1]:

$$\frac{\partial N_i}{\partial t} - \nabla \cdot (\hat{D}_i \nabla N_i) + \frac{\partial}{\partial E_k}(b_i N_i) + nv\sigma_i N_i + \frac{1}{\tau_i} N_i = q_i + \sum_{j>i} nv\sigma_{ij} N_j + \sum \frac{1}{\tau_{ij}} N_j. \tag{1}$$

The second term characterises the diffusion in the galactic magnetic field inhomogeneities, where $\hat{D}_i(\vec{r}, E_k)$ is the diffusion tensor. The third term represents the continuous energy losses, in particular ionisation losses, where $b_i(\vec{r}, E_k) = \frac{\mathrm{d}E_k}{\mathrm{d}t}$ is the energy change of an individual particle per unit of time. This term can be neglected for energies $E_k \gtrsim 500\,\mathrm{GeV/n}$. $nv\sigma_i N_i$ and $\sum_{j<i} nv\sigma_{ij} N_j$ are the absorption term of the particle i and the production term of the particle i from the heavier parent particle j, where $n(\vec{r})$ is the density of the interstellar gas, v the velocity of the nucleus, $\sigma_i(E_k)$ the inelastic scattering cross section of a nucleus i and $\sigma_{ij}(E_k)$ the production cross section of a nucleus i from a heavier particle j. $\frac{1}{\tau_i} N_i$ and $\sum \frac{1}{\tau_{ij}} N_j$ take into account the disappearance by radioactive decay of the nuclei i and respectively the apparition of the nuclei j via radioactive decay of the species i. The accelerated particles, originating from point-like sources, and their power are described by the functions $q_i(t, \vec{r}, E_k)$. This is the source term, which is zero for secondary nuclei.

1.3.2 Galactic wind

Cosmic rays may not only diffuse in our Galaxy, because it is possible that they can also be carried by a "frozen" magnetic field in form of magnetohydrodynamic waves. With convection of the velocity $\vec{V}_c(t, \vec{r})$ equation (1) has the following form (ionisation losses are neglected) [1]:

$$\frac{\partial N_i}{\partial t} - \nabla \cdot (\hat{D} \nabla N_i) + \nabla \cdot (\vec{V}_c N_i) - \frac{\nabla \cdot \vec{V}_c}{3} \frac{\partial}{\partial E_k} \left(\frac{2mc^2 + E}{mc^2 + E} E_k \right) + nv\sigma_i N_i + \frac{1}{\tau_i} N_i = q_i + \sum_{j>i} nv\sigma_{ij} N_j + \sum \frac{1}{\tau_{ij}} N_j, \tag{2}$$

where the third term corresponds to the convection provoked by the galactic wind and the fourth term represents the adiabatic expansion. It is connected with a change in the energy of the particles in flows with $\nabla \cdot \vec{V}_c \neq 0$. A characteristic value of the convection velocity is $20\,\mathrm{km \cdot s^{-1}}$.

1.3.3 Reacceleration [6, 7]

We have seen that the propagation of cosmic rays could be much more complex as the "simple" diffusion model, if charged particles interact with magnetohydrodynamic waves. There exist two arguments which lead to consider a reacceleration of cosmic-ray particles. The first is connected to magnetic field inhomogeneities, which conduct naturally to an energy gain by Alfvén waves. The second argument is more an experimental one. The ratio of secondary-to-primary nuclei falling rapidly with increasing energy favours a reacceleration.

There are two different types of reacceleration:

Distributed reacceleration: The acceleration is prompt and "on-off" (i.e. supernova explosion).

Diffusive reacceleration: The acceleration is continuous and due to the magnetic field inhomogeneities.

The main difference between the two processes are that the first is discrete and the second is continuous. The second allows a treatment of a second order Fermi acceleration, because of the small energy gain in a single collision, using the Fokker-Planck formalism. From another point of view, we can start with a collisionless Boltzmann equation and expand it up to second order in disturbed quantities, i.e. magnetic irregularities [7]. We will look now closer at this second method.

The momentum spectrum of particles undergoing Fermi acceleration due to irregularly moving magnetized fluid elements is studied in terms of a diffusion equation in momentum space provided that the hydromagnetic turbulence may be regarded as homogeneous and time-independent [7]:

$$\frac{\partial f}{\partial t} = \frac{1}{p^2}\frac{\partial}{\partial p}\left[p^2 D(p)\frac{\partial f}{\partial p}\right]. \tag{3}$$

If we idealise the magnetised fluid elements as hard spheres with masses much larger than those of the particles, the diffusion coefficient, $D(p)$, is given for an elastic collision as

$$D(p) = \frac{V_a^2}{3lc\beta}p^2, \tag{4}$$

where V_a and $c\beta$ are the velocities of the fluid elements (Alfvén velocity) and particles, respectively, whereas l is the particles mean free path against collisions with the fluid elements. The Alfvén velocity represents in general the velocity by which a perturbation in the magnet field could propagate along the magnetic field lines. Expressing the latter quantity in terms of the spatial diffusion coefficient, $K = \frac{1}{3}lc\beta$, gives

$$D(p) = \frac{V_a^2 p^2}{9K}. \tag{5}$$

1.3.4 Full diffusion equation

If we consider now all the phenomena seen in the sections above, i.e. convection and reacceleration, the initial diffusion equation (1) becomes:

$$\begin{aligned}\frac{\partial N_i}{\partial t} - \nabla\cdot(D_{xx}\nabla N_i) + \nabla\cdot(\vec{V}_c N_i) + \frac{\partial}{\partial E_k}(b_i N_i) - \frac{\nabla\cdot\vec{V}_c}{3}\frac{\partial}{\partial E_k}\left(\frac{2mc^2+E}{mc^2+E}E_k\right) + nv\sigma_i N_i + \frac{1}{\tau_i}N_i = \\ q_i + \frac{1}{p^2}\frac{\partial}{\partial p}\left[p^2 D_{pp}\frac{\partial N_i}{\partial p}\right] + \sum_{j>i} nv\sigma_{ij}N_j + \sum\frac{1}{\tau_{ij}}N_j,\end{aligned} \tag{6}$$

where D_{xx} and D_{pp} are the spatial and the momentum diffusion coefficients respectively, with $D_{pp} = \frac{V_a^2 p^2}{9D_{xx}}$, V_a the Alfvén velocity, and V_c the convection velocity.

1.3.5 Some custom models

Resolving the diffusion equation (1) requires the complete analysis of a system of coupled equations. For this we have to assume that all the parameters are well known and we need to know the form and the size of the propagation region of cosmic rays in the Galaxy, as well as the distribution of the interstellar gas and of the sources. We do not have all the information for resolving the equation system, but there exist models, approximating the solution with some assumptions. We want to present here in this section the Leaky Box model, which is one of the most used models, and the weighted slab model.

Leaky Box Model

The Leaky Box model, introduced in the 60th, is as an extremely simplified version of the diffusion model, in which we assume that diffusion takes places rather rapidly: the distribution of cosmic rays in the whole box (i.e. Galaxy) is homogenous and in contrary it is necessary to allow a certain escape time of cosmic rays from the system. Starting from equation (1) with the substitution

$$-\nabla\cdot(\hat{D}_i\nabla N_i) \qquad \longleftrightarrow \qquad \frac{N_i}{\tau_{\text{esc}}},$$

where τ_{esc} is the escape time of cosmic rays from the Galaxy, and with the average of every quantity:

$$n \longleftrightarrow \bar{n} \qquad \text{and} \qquad q \longleftrightarrow \bar{q},$$

we obtain [1] [6], if we neglect the radioactive nuclei and ionisation losses:

$$\frac{N_i}{\tau_{\rm esc}} + \bar{n}v\sigma_i N_i = q_i + \sum_{j>i} \bar{n}v\sigma_{ij} N_j. \tag{7}$$

The resulting system of equations for the various kinds of nuclei i are purely algebraic. The characteristic escape time $\tau_{\rm esc}$ is principally determined by experiments and purely phenomenological. We can see that this simple model permits a direct analysis of flux measurements in function of only three parameters: the escape time, the mean matter density and the abundance sources. But this model is only an approximation which does not give us an indication of the many physical processes. In contrary this model is sufficient for our use, because it reproduces the found experimental data for secondary-to-primary ratios.

Weighted Slab Model [1] [6, 8]

The principal idea of weighted slab model is to choose a geometry for the Galaxy and to replace the time and space dependence of the fluxes with a dependance of the matter thickness traversed.

We look for a stationary ($\frac{\partial N_i}{\partial t} = 0$) solution for this model of the form

$$N_i(\vec{r}, E_k) = \int_0^\infty N_i^{\rm WSM}(x, E_k) G(\vec{r}, x, E_k) {\rm d}x, \tag{8}$$

where the function G corresponds to the path length distribution. This parameter gives the probability for a nuclei at a position $\vec{r}$ of traversing the thickness x during its propagation. This probability is normalised

$$\int_0^\infty G(x){\rm d}x = 1.$$

The average thickness of the traversed matter by a nucleus is equal to

$$\bar{x} = \int_0^\infty xG(x){\rm d}x.$$

The functions $N_i^{\rm WSM}(x)$ are the cosmic-ray flux, when it has traversed a matter slab of thickness x and are determined from the system of equations

$$\frac{{\rm d}N_i^{\rm WSM}(x)}{{\rm d}x} = \frac{1}{\bar{m}} \left(\frac{q_i}{nv} + \sum_{j>i} \sigma_{ij} N_j(x) - \sigma_i N_i(x) \right) \quad \text{or} \tag{9}$$

$$\frac{{\rm d}N_i^{\rm WSM}(x)}{{\rm d}x} = \frac{1}{\bar{m}} \left(\sum_{j>i} \sigma_{ij} N_j(x) - \sigma_i N_i(x) \right) \quad \text{with the initial condition} \tag{10}$$

$$N_i^{WSM}(0) = q_j(E),$$

where $\bar{m}$ is the average ISM mass. These equations are quite general and applicable for every model, because the function $G(x)$ is not yet defined, and they could be resolved analytically.

By neglecting the energy losses and radioactive nuclei, the energy E_k remains in the equations as a parameter, equation (1) takes the form

$$\frac{\partial N_i}{\partial t} - \nabla \cdot (\hat{D}_i \nabla N_i) + nv\sigma_i N_i = q_i + \sum_{j>i} nv\sigma_{ij} N_j. \tag{11}$$

If we insert equation (8) in equation (11) for obtaining an equivalent formula to equation (1) we find that G does satisfy the equation

$$nv\frac{\partial G}{\partial x} - \nabla \cdot (\hat{D} \nabla G) = f(r,t)\delta(x), \tag{12}$$

where $f(r,t)$ is the spacial source distribution.

At the high-energy limit and for diffusion coefficients which do not depend on the considered cosmic-ray type, the solution of equations (8) and (10) is strictly equivalent to the direct solution of the diffusion equation (1). This model is adapted for every geometrical model of our Galaxy and for all spatial source distributions. This model, easy to resolve and largely used, permits to have results for the radioactive nuclei and can contain a little bit more physics as the Leaky Box model. We will use this model for the cosmic-ray propagation in the Earth's atmosphere.

1.4 Solar Modulation and fluxes on the top of the atmosphere

We have seen that the energy spectrum of cosmic rays is modulated for energies up to several GeV/n. This is due to a phenomenon called the solar wind. In the 1950s, a German scientist named Ludwig Biermann became interested in the fact that no matter whether a comet is headed towards or away from the Sun, its tail always points away from the Sun. Biermann postulated that this happens because the Sun emits a steady stream of particles that pushes the comet's tail away. In fact a fully ionised gas, thus a plasma, basically constituted of protons and electrons with an energy around 500 keV, is pushed radially out of the Sun's corona. Once the plasma has left the solar corona, the dynamic pressure of the wind dominates over the magnetic pressure through most of the solar system, so that the magnetic field is pulled into an Archimedean spiral pattern (the Parker spiral) by the combination of the outward motion and the Sun's rotation [10].

The charged particles of the cosmic rays are diffused and energetically influenced (slow down) by this magnetic field. This influence can be calculated by an equation based on a convection-diffusion model [11]:

$$\frac{\partial U}{\partial t} + \frac{1}{r^2}\frac{\partial}{\partial r}(r^2 V U) - \frac{1}{r^2}\frac{\partial}{\partial r^2}\left(r^2 \kappa \frac{\partial U}{\partial r}\right) - \frac{1}{3r^2}\left[\frac{\partial}{\partial r}(r^2 V)\right]\left[\frac{\partial}{\partial T}(\alpha T U)\right] = 0, \tag{13}$$

where

$$\alpha = \frac{T + 2mc^2}{T + mc^2}.$$

Here $U(r, T)$ is the differential density r the radial distance from the Sun, $V(r, t)$ the solar-wind speed, κ the diffusion coefficient, T the kinetic energy and m the mass of the considered particle. This equation describes the effects of convection (first term in (13)) and scattering of cosmic-ray particles by "magnetic scattering centres" (second term) carried along by a radially moving solar wind, with the assumption of spherical symmetry. The third term describes the adiabatic expansion. The steady state equation (with $\frac{\partial U}{\partial t} = 0$) is well appropriate since the duration of direct detection experiments like CREAM (1-3 months) and AMS02 (three years) are short in comparison to the 11 year period of the solar cycle.

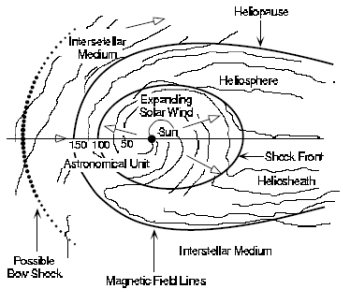

(a) A schematic view of the heliosphere and its interaction with the interstellar medium [12].

(b) Heliospheric current sheet, the largest structure in the Solar System, resulting from the influence of the Sun's rotating magnetic field on the plasma in the interplanetary medium (Solar Wind) from the NASA artist Werner Heil.

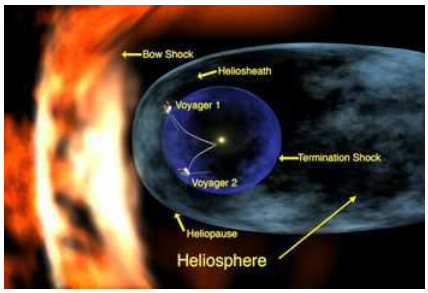

(c) This shows the locations of Voyagers 1 and 2. Voyager 1 has crossed into the heliosheath, the region where interstellar gas and solar wind start to mix [13].

1.4.1 Force field solar modulation

One method to resolve equation (13) is the approximation of a force field. The idea is to make an analogy to a radial electric field with a potential ϕ. In this approximation the equation of density evolution is:

$$\kappa \frac{\partial U}{\partial r} + \frac{V}{3}\left(T^2 - (mc^2)^2\right)^{3/2}\frac{\partial U}{\partial (T)}\left[\frac{U}{T\left(T^2 - (mc^2)^2\right)^{1/2}}\right] = 0. \tag{14}$$

This equation can be regarded as an asymptotic solution of the correct equation (13) valid at high energies. With a given κ this equation can be integrated. After the application of the boundary conditions the changes of the cosmic ray flux $J(E) = \frac{vU(E)}{4\pi}$ can be expressed as follows (for more details see reference [11]):

$$J_{\mathrm{mod}}(E) = \frac{E^2 - m^2c^4}{(E + Ze\phi)^2 - m^2c^4} J(E + Ze\phi), \tag{15}$$

with the particle charge Z in units of electrical charge e, and ϕ, which depends itself on the solar wind velocity V, the radial diffusion coefficient $k = \frac{\kappa}{\beta R}$, where $R = \frac{pc}{Ze}$ is the rigidity and $\beta = \frac{v}{c}$ the particle velocity, and on the "modulation boundary" r_b (influence zone of the solar wind). ϕ is given by the equation

$$\phi(r,t) = \int_r^{r_b} \frac{V}{3k}\,\mathrm{d}x = \frac{V(r_b - r)}{3k}.$$

We can give some values of the different parameters:

k		depends on the solar period
r_b	$=$	$100\,\mathrm{AU}$
V	$\approx$	$400\,\mathrm{km \cdot s^{-1}}$
R	$\approx$	$1\,\mathrm{GV}$
ϕ	$\approx$	$250 - 750\,\mathrm{MV}$ for the solar minimum and maximum, respectively

It is very important to be aware of the solar modulation. This permits to infer the fluxes on the top of the atmosphere from the interstellar cosmic-ray fluxes.

1.4.2 Top of the atmosphere (TOA) and interstellar (IS) fluxes

The solar modulated cosmic ray fluxes are also known as the top of atmosphere (TOA) fluxes, which are in fact the individual cosmic-ray element spectra, which we measure on the top of the Earth's atmosphere, but which do not correspond to the interstellar cosmic-ray fluxes. Experiments, detecting cosmic rays, can extrapolate the TOA fluxes, but have to consider the solar modulation to obtain the flux of interstellar cosmic rays.

Wiebel-Sooth, Biermann & Meyer (see reference [14]) have fitted the basic data set for interstellar cosmic ray fluxes above $10\,\mathrm{GeV/n}$, where the solar modulation is negligible, as available in the literature, of the form

$$\phi(E) = \phi_0 \left(\frac{E}{\mathrm{TeV}}\right)^{-\gamma} (\mathrm{m^2\,sec\,sr\,TeV})^{-1}, \tag{16}$$

where E is the energy per particle. The results for particles with charge Z are given in table 1. Because GeV/n is the current unit for the cosmic ray differential fluxes, we transformed this equation to the following:

$$\phi_n(E_n) = A \cdot 10^{-3}\phi_0 \left(A \cdot 10^{-3}\frac{E_n}{\mathrm{GeV/n}}\right)^{-\gamma} (\mathrm{m^2\,sec\,sr\,GeV/n})^{-1} \tag{17}$$

where E_n is the energy per nucleon. The modulated fluxes are deduced from the interstellar fluxes ϕ_n as described in section (1.4.1).

1.5 Physics of cosmic rays

Cosmic rays are used to infer useful properties about our Galaxy, such as its composition, its basic structure (homogeneity of the Galaxy, existence of an extended halo), and what common physical processes occur within the Galaxy (acceleration and propagation of the particles, etc). By identifying the different nuclei we hope to be able to unreveal the production mechanism (nucleosynthesis in stars and supernova) and fragmentation processes of cosmic rays.

1.5.1 Dark matter

During their propagation, cosmic rays interact with the interstellar medium and with the solar wind, producing a lot of different particles and antiparticles. The observation of antiproton, positron, antideuton, and photon spectra permits, through an excess production of these, a search for supersymmetric dark matter candidates, like the Weakly Interacting Massive Particle (WIMP, χ), through their annihilation and decay products in the galactic halo.

$$\begin{aligned} \chi + \bar{\chi} &\longrightarrow \bar{p} + X, e^+ + X, \bar{D} + X, 2\gamma \\ \chi, \bar{\chi} &\longrightarrow \gamma\nu \end{aligned}$$

Element	Z	ϕ_0	γ	χ^2/df
H	1	$(11.51 \pm 0.41) \cdot 10^{-2}$	2.77 ± 0.02	0.70
He	2	$(7.19 \pm 0.20) \cdot 10^{-2}$	2.64 ± 0.02	2.63
Li	3	$(2.08 \pm 0.51) \cdot 10^{-3}$	2.54 ± 0.09	0.90
Be	4	$(4.74 \pm 0.48) \cdot 10^{-4}$	2.75 ± 0.04	0.37
B	5	$(8.95 \pm 0.79) \cdot 10^{-4}$	2.95 ± 0.05	0.45
C	6	$(1.06 \pm 0.01) \cdot 10^{-2}$	2.66 ± 0.02	1.42
N	7	$(2.35 \pm 0.08) \cdot 10^{-3}$	2.72 ± 0.05	1.91
O	8	$(1.57 \pm 0.04) \cdot 10^{-2}$	2.68 ± 0.03	1.70
F	9	$(3.28 \pm 0.48) \cdot 10^{-4}$	2.69 ± 0.08	0.47
Ne	10	$(4.60 \pm 0.10) \cdot 10^{-3}$	2.64 ± 0.03	3.14
Na	11	$(7.54 \pm 0.33) \cdot 10^{-4}$	2.66 ± 0.04	0.36
Mg	12	$(8.01 \pm 0.26) \cdot 10^{-3}$	2.64 ± 0.04	0.10
Al	13	$(1.15 \pm 0.15) \cdot 10^{-3}$	2.66 ± 0.04	1.24
Si	14	$(7.96 \pm 0.15) \cdot 10^{-3}$	2.75 ± 0.04	0.10
P	15	$(2.70 \pm 0.20) \cdot 10^{-4}$	2.69 ± 0.06	0.68
S	16	$(2.29 \pm 0.24) \cdot 10^{-3}$	2.55 ± 0.09	0.44
Cl	17	$(2.94 \pm 0.19) \cdot 10^{-4}$	2.68 ± 0.05	2.36
Ar	18	$(8.36 \pm 0.38) \cdot 10^{-4}$	2.64 ± 0.06	0.45
K	19	$(5.36 \pm 0.15) \cdot 10^{-4}$	2.65 ± 0.04	4.58
Ca	20	$(1.47 \pm 0.12) \cdot 10^{-3}$	2.70 ± 0.06	0.60
Sc	21	$(3.04 \pm 0.19) \cdot 10^{-4}$	2.64 ± 0.06	0.81
Ti	22	$(1.13 \pm 0.14) \cdot 10^{-3}$	2.61 ± 0.06	5.67
V	23	$(6.31 \pm 0.28) \cdot 10^{-4}$	2.63 ± 0.05	6.83
Cr	24	$(1.36 \pm 0.12) \cdot 10^{-3}$	2.67 ± 0.06	3.41
Mn	25	$(1.35 \pm 0.14) \cdot 10^{-3}$	2.46 ± 0.22	5.38
Fe	26	$(1.78 \pm 0.18) \cdot 10^{-2}$	2.60 ± 0.09	1.81
Co	27	$(7.51 \pm 0.37) \cdot 10^{-5}$	2.72 ± 0.09	1.13
Ni	28	$(9.96 \pm 0.43) \cdot 10^{-4}$	2.52 ± 0.18	5.47

Table 1: Individual element spectra [14]

1.5.2 Constraints on the propagation parameters [1]

Knowing the abundances of the various kinds of secondary nuclei, produced via spallation while propagating through the interstellar medium, we can determine several parameters of the propagation of cosmic rays in the Galaxy. This allows us to restrict some cosmic-ray propagation models. For example, diffusive reacceleration contributes significantly in shaping the boron-to-carbon (B/C) ratio at kinetic energies per nucleon around $1\,\mathrm{GeV/n}$.

Stable nuclei

In the Leaky Box model, in the case of known cross sections, the relative abundance of stable secondary nuclei is completely determined by the average thickness of matter $\lambda_{\mathrm{esc}} = \bar{n} v \tau_{\mathrm{esc}}$ [cm^{-2}] traversed by the particles. Knowing the densities of some kinds of secondary nuclei N_i, we can find the value of λ_{esc} from:

$$\lambda_{\mathrm{esc}} = \left[\left(\sum_{j>i} \sigma_{ij} \frac{N_j}{N_i} \right) - \sigma_i \right]^{-1} . \tag{18}$$

From the abundances of the light nuclei and the nuclei of the sub-Fe group at energies $1 - 3\,\mathrm{GeV/n}$ the value $\lambda_{\mathrm{esc}} \approx 3 - 5 \cdot 10^{24}\,\mathrm{cm}^{-2}$ or $\bar{\lambda}_{\mathrm{esc}} = \bar{m}\lambda_{\mathrm{esc}} \approx 5 - 8\,\mathrm{g\,cm}^{-2}$ is found [1].

The Leaky Box model gives also a phenomenological form of the dependence of the particle rigidity $R = p/Z$ on the grammage, describing the observed ratio B/C:

$$\begin{cases} \bar{\lambda}_{\mathrm{esc}} = \bar{\lambda}_0 \beta, & \text{if } R < R_c \\ \bar{\lambda}_{\mathrm{esc}} = \bar{\lambda}_0 \beta \left(\dfrac{R}{R_c} \right)^{-\delta}, & \text{if } R > R_c \end{cases} \tag{19}$$

where $\bar{\lambda}_0 = 24\,\mathrm{g\,cm}^{-2}$. This parametrisation is valid for particles in the interstellar medium with energies from about $0.4 - 300\,\mathrm{GeV/n}$ where data on secondary nuclei are available [9].

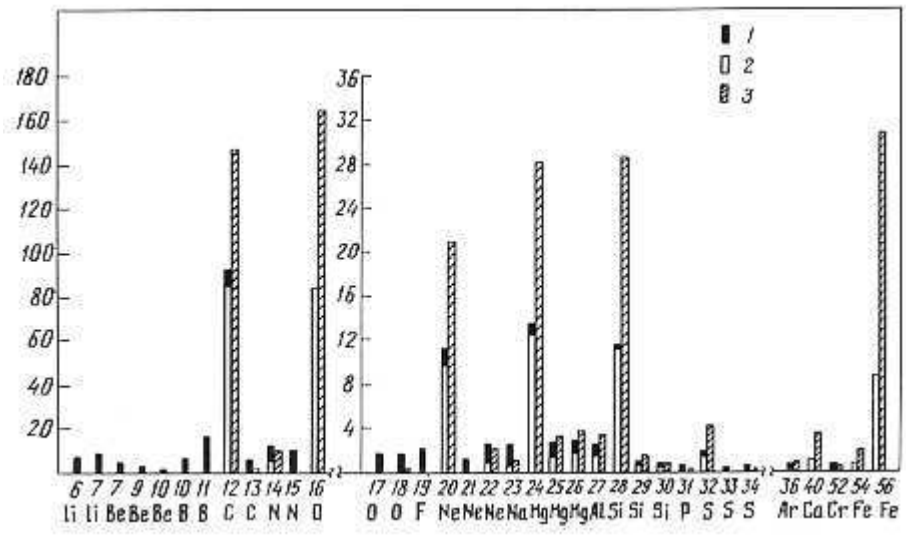

Figure 4: The fractions of secondary (1) and primary (2) nuclei in the cosmic rays on Earth, and the abundance of the various nuclei in the cosmic ray sources (3) [1]

Determining the parameters for the diffusion model is much more complicated as for the Leaky Box model. But the one-dimensional diffusion and the Leaky Box models are equivalent under some assumptions and their parameters are related by the relation:

$$\lambda_{\rm esc} = \frac{nvhL}{D} \qquad \left(\frac{h}{L} \ll 1\right),$$

which is valid under the condition

$$\lambda_{\rm esc} \cdot \sigma \ll \frac{L}{h},$$

where σ is the total fragmentation cross section of the heaviest of the nuclei under consideration, h the galactic disk size and L the halo size.

The physical interpretation of the empirical equation (19) for $R > R_c$ can be given in the framework of the diffusion model. The theory of particle resonant scattering and diffusion in the turbulent interstellar medium predicts the scaling of the diffusion coefficient [9]:

$$D = D_0 \beta R^{\delta}, \tag{20}$$

where D_0 is the normalisation of the diffusion coefficient, which is linked to the level of the hydromagnetic turbulence and expressed in $\mathrm{cm}^2\,\mathrm{s}^{-1}$. The diffusion coefficient spectral index δ is linked to the density spectrum of these irregularities at different wavelengths. The Kolmogorov theory for the turbulence spectrum predicts $\delta = 1/3$, while fits to the B/C ratio within the diffusion model of equation (6) at MeV and GeV energies prefer high values for δ ($\sim 0.5 - 0.7$). We can see, that the B/C ratio is a good test for some propagation models through a fit of the spectral index δ.

Radioactive nuclei

Secondary stable nuclei give important information on the parameters of propagation models of cosmic rays in the interstellar medium, but they do not make it possible to determine the time that the particles remain in the Galaxy. We can determine the age of the cosmic rays from the relative content of radioactive nuclei.

In the frame of the Leaky Box model, equation (7) for secondary radioactive nuclei of type i neglecting ionisation losses takes the form (decays of the other nuclei are not taken into account)

$$\left(\frac{1}{\lambda_{\rm esc}} + \sigma_i + \frac{1}{\bar{n} v \gamma \tau_i}\right) N_i = \sum_{j>i} \sigma_{ij} N_j. \tag{21}$$

We consider here two secondary isotopes, produced by the same primary cosmic ray P, where one is radioactive R and the other is stable S. For simplifying we make the approximation that $\sigma_{RP} = \sigma_{SP} = \sigma_{iP}$ for the

fragmentation cross sections and $\sigma_R = \sigma_S = \sigma_i$ for the total inelastic cross sections, where i signifies here the chosen secondary element. Equation (18) (in the form of equation (21)) and equation (21) become equivalent and they allow us to determine the average density $\bar{n}$ of the gas in the propagation region and the escape time of the cosmic rays from the Galaxy,

$$\tau_{\text{esc}} = \frac{\lambda_{\text{esc}}}{\bar{n}v} :$$

$$\bar{n} = \frac{\frac{N_R}{N_S}}{1 - \frac{N_R}{N_S}} \frac{\lambda_{\text{esc}}}{(1 + \sigma_i \lambda_{\text{esc}}) v \tau_i} \tag{22}$$

$$\tau_{\text{esc}} = \frac{1 - \frac{N_R}{N_S}}{\frac{N_R}{N_S}} (1 + \sigma_i \lambda_{\text{esc}}) \tau_i. \tag{23}$$

Here N_R and N_S are the abundances of the radioactive and stable nuclei of the element i, and τ_i the life time of the radioactive isotope i.

1.6 Detection of cosmic rays

Direct measurements of primary cosmic-ray energy spectra and of their elemental composition up to the highest energies are the goals of a series of experiments planned to take data in the next years. The aim is to understand the so far unknown mechanism of acceleration of primary cosmic rays of very high energy, to identify their sources and to clarify their interactions with the intergalactic medium. Since the discovery of cosmic rays the experiments for its detection have quickly improved and are nowadays very diversified. We have seen in section 1.2.1 that the cosmic-ray particle flux decreases with energy in form of a power law, which means that a direct detection of the cosmic-ray particles for energies above $\approx 10^{14}$ eV is no more possible. Therefore, measurements are divided into two classes:

direct detection of primary cosmic rays by space-based and balloon experiments in the energy range of $10^3 - 10^{14}$ eV,

indirect detection by ground-based air shower experiments for the energies $10^{13} - 10^{20}$ eV, which observe the extensive showers of secondary particles initiated when a primary cosmic ray interacts with a nucleus of the upper atmosphere.

In this section we will discuss several aspects of direct and indirect detection methods and different conceptions of experiments for the two detection types. A great number of cosmic-ray experiments exists, which can not be listed here. We will present shortly four different experiments, each covering a given energy range representing the different measurement techniques and scientific goals.

1.6.1 Direct detection [15]

The direct detection of primary cosmic rays is assured by balloon and space-based experiments. We start with the description of balloon experiments and its conception. Balloons with a volume of one million cubic metres are able to bring three ton payloads up to an altitude of around 40 km. At this altitude the atmospheric grammage is $3 - 5\,\text{g/cm}^2$, which is close to the space conditions. The typical flight time is around 30 hours, but this depends on the weather, wind and the balloon conditions. An additional limiting factor is that the balloon looses altitude by night. For a longer flight duration the possibility exists to fly for 40 days around the pole, due to the circumpolar wind during the antarctic summer, when it is always bright. But this possibility reduces the maximum payload to the half and increases the risk of a total experiment loss. To arise the flight duration NASA works actually on Ultra Long Duration Balloons (ULDB) which is a pumpkin-shaped superpressure balloon designed for durations up to 100 days [16].

A balloon flight mission is relatively simple. The balloon is partially filled with helium and launched with the payload suspended beneath it. As the balloon rises, the helium expands and fills out the balloon until it reaches its float altitude two to three hours after launch. Once the scientists have concluded the experiment, a radio command is sent from a ground station or a chase plane to separate the payload from the balloon. Payload separation creates a tear in the balloon, which releases the gas. The parachute opens and floats the payload back to the ground so it can be reused. The payload reaches the ground about 45 minutes after it has been separated from the balloon. The balloon material falls to the ground, where it is retrieved and discarded.

The limits of balloon experiments are reached when the cosmic-ray particle flux is too small for registering enough events during the flight duration and when the upper atmosphere highly disturbs the measurements. In

this case only satellites and space stations can be used. For this a magnetic spectrometer is one option. Until now only two magnetic spectrometers have been flown in space: the MARIYA experiment on the Russian space station MIR and the AMS-01 experiment on the NASA space shuttle Discovery.

1.6.2 Experiments

We will introduce the space-based experiment AMS, which will study cosmic rays and especially will look for dark matter and antimatter and will enlarge the elemental cosmic-ray spectrum measurements to high energies. The second direct cosmic-ray detector is the balloon experiment CREAM which will allow with the collected data to measure the diffusion coefficient spectral index δ and to constrain the other propagation parameters.

AMS [17]

The Alpha Magnetic Spectrometer (AMS) is a space-born detector for cosmic rays built from an international collaboration, that will be operated aboard of the International Space Station for at least 3 years, collecting several billions of high-energy protons and nuclei. Its main goal is the search for dark matter and antimatter. In addition, by extending measurements of beryllium isotopes to high energies ($2-8\,\mathrm{GeV/nucleon}$) AMS can distinguish between current models of cosmic ray transport.

In its first configuration (known as AMS-01), it was installed on the shuttle Discovery, that during the STS-91 mission (2 - 12 June 1998) carried it along an orbit similar to that of the ISS. During the 10 days of this trial mission, AMS acquired data corresponding to approximately 100 millions of triggers, letting us understand how well it will behave on the ISS.

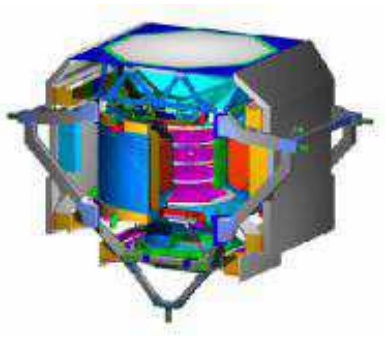

Figure 5: Schematic of the AMS instrument configuration

Following the precursor flight data analysis, a major upgrade of the detector has been proposed (called AMS-02 in the following), based on a superconducting magnet and on the addition of various detectors (Transition radiation detector - TRD, Ring Imaging Cherenkov detector RICH, Electromagnetic Calorimeter - ECAL). The upgrade will allow AMS to extend the particle measurements and identification to very high energies.

AMS-01 The AMS-01 detector is based on a permanent Ne-Fe-B magnet with an analyzing power of $0.15\,\mathrm{T\,m^2}$ that contains 4 of the 6 layers of the Silicon tracker and the scintillator counters of the anticoincidence system. Each tracker plane gives a measure of 2 coordinates (x, y) with a resolution of 30 (x) and 10 (y) microns and of energy deposition, thus giving the particle momentum and charge.

The trigger is given by the time of flight (TOF) system, that in addition measures the velocity of the traversing particles and their charge. Combined to the tracker measurements, this allows the determination of the particle mass. The detector is completed with a threshold Cherenkov counter, below the magnet, to improve the separation between electrons and protons up to $3.5\,\mathrm{GV}$.

AMS-02 During the years spent on the International Space Station, AMS will have a different configuration from that of the STS-91 flight. The magnet will be a superconducting one, and the tracker will have 8 Si planes, to achieve better rigidity resolution, there will be a RICH to extend to higher energies the Time Of Flight(TOF) measurement range, and a TRD and an electromagnetic calorimeter will improve the capability to distinguish between different particles.

CREAM [18]

The Cosmic Ray Energetics And Mass (CREAM) project will investigate ultra high-energy (10^{12} to $> 5 \cdot 10^{14}$ eV) cosmic rays over the elemental range from protons to iron utilising a series of Ultra Long Duration Balloon (ULDB) flights. The goal is to observe spectral features and/or abundance changes that might be related to a supernova acceleration limit. The measurements will be made with an instrument consisting of a sampling tungsten/scintillating-fiber calorimeter preceded by a graphite target with scintillating-fiber layers for trigger and track-reconstruction purposes, a transition radiation detector (TRD) for observing heavy nuclei, and a segmented timing-based particle-charge detector. A key feature of the instrument is its ability to obtain simultaneous measurements of the energy and charge of a subset of nuclei by the complementary calorimeter and TRD techniques, thereby allowing in-flight inter-calibration of their energy scales. The energy reach will depend on a series of ULDB flights of identical instruments: three flights will reach $5 \cdot 10^{14}$ eV. The different flights can be carried out at essentially any latitude, including the polar regions of either hemisphere.

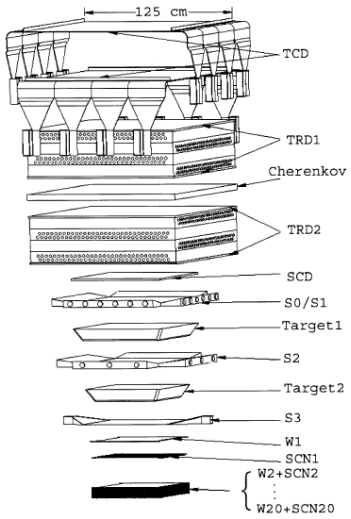

Figure 6: Schematic of the CREAM instrument configuration

CREAM was launched for the first time from the National Science Foundation's McMurdo Station, Antarctica on December 16, 2004. The balloon travelled 41 days and 22 hours. It landed on January 27, 660 kilometers from McMurdo Station after making three orbits around the South Pole. CREAM broke the flight record for duration and distance. The second flight of the detector began on December 15, 2005 and it landed on January 13, 2006 after a flight of 28 days and 10 hours. A third flight is planned for December 2007.

1.6.3 Indirect detection

The indirect detection of cosmic rays is based on the observation of extensive air showers with ground-based experiments. An extensive air shower is the phenomenon where multiple generations of secondary cosmic rays are produced when primary cosmic rays interact with atoms in the upper atmosphere, yielding subatomic particles and gamma rays. The secondary cosmic rays in turn produce even more down through the atmosphere. Billions of these particles travel downward at nearly the speed of light and at ground level may extend over several square kilometres. The maximum flux of cosmic rays, both primary and secondary, is at an altitude of 20 km, and below this the absorption by the atmosphere reduces the flux.

The primary cosmic ray interacts with several nucleons of the atmospheric nucleus. This produces predominately pions, but also strange particles (K, ...) or antinucleons. These secondary products cause also hadronic interactions until the energy falls below the necessary energy for pion production, hence below circa 1 GeV. Such a reaction chain is called hadronic cascade.

Another possibility, in addition, for further interactions is the decay of the particle. Pions for example predominantly decay to

$$\begin{aligned} \pi^0 &\longrightarrow 2\gamma \\ \pi^+ &\longrightarrow \mu^+\nu_\mu \\ \pi^- &\longrightarrow \mu^-\bar{\nu}_\mu \end{aligned}$$

The pion cascade produces thus high energetic photons, muons and neutrinos. The muons decay to

$$\begin{aligned} \mu^+ &\longrightarrow e^+\nu_e\bar{\nu}_\mu \\ \mu^- &\longrightarrow e^-\bar{\nu}_e\nu_\mu \end{aligned}$$

In addition the photons produce through pair production e^+e^--pairs and these through Bremsstrahlung again photons. It comes to a formation of an electromagnetic cascade.

A complete air shower consists of three components: the electromagnetic, muonic, and hadronic component. A primary proton with an energy of 10^{15} eV produces about 10^6 secondary particles (80% photons, 18% electrons and positrons, 1.7% muons and 0.3% hadrons).

Three types of experiments are applied for indirect detection:

- Air-Čerenkov-technique,
- particle shower detection by detector arrays and

- muon and neutrino detection in underground laboratories.

Čerenkov-technique: Čerenkov light is emitted when the velocity of a charged particle is greater than the speed of light in a medium with a given refractive index n:

$$v > \frac{c}{n}.$$

A typical Čerenkov cone, produced in an altitude between 7 and 20 km, has a radius of about 150 m. The number of the Čerenkov photons for a primary particle with an energy of 1 TeV amounts to about 10^6. The detection of these photons is made by photomultipliers. A disadvantage of this technique is, that the observation can only be made during moonless nights.

Detector arrays: To get a good signal of a primary cosmic-ray particle at sea level, it must have an energy of circa 0,1 PeV. For the observation of extensive air showers one uses a great number of detectors (more than 100), which are distributed over a great area (typically 1 km^2). These detectors are scintillator counters. Due to the chronology and the deposited energy in each counter, one can get information about the direction and the energy of the primary cosmic ray particle. Also the separate measurement of the muon shower component is from great interest. The ratio of muons to electrons permits to identify the composition of the primary cosmic rays at very high energy.

Fluorescence-technique: The charged particles in an air shower also interact with atmospheric nitrogen, causing it to emit ultraviolet light (300-400 nm) via a process called fluorescence. The basic function of the fluorescence detectors is to measure the longitudinal profile of the extensive air showers. The light collection via e.g. mirrors can only be done in moonless nights.

1.6.4 Experiments

The two experiments we would like to present are the two biggest EAS experiments actually existing: the KASCADE experiment and the Pierre Auger Observatory. These experiments are looking for the two "holy grails" of astroparticle physics: the knee for KASCADE and the ankle for Auger.

KASCADE [19]

The KArlsruhe Shower Core and Array DEtector-Grande (KASCADE-Grande) is an extensive air shower experiment to study the cosmic-ray primary composition and hadronic interactions in the energy range $E = 10^{14} - 10^{18}$ eV. The experiment is situated on site of the Forschungszentrum Karlsruhe in Germany. It measures simultaneously the electromagnetic, muonic, and hadronic components of extensive air showers. As an extension of the former KASCADE experiment running successfully since 1996, KASCADE-Grande was built by reassembling 37 stations of the former EAS-TOP experiment – basically the electromagnetic detectors – running between 1987 and 2000 at Campo Imperatore, Grand Sasso Loboratories, Italy.

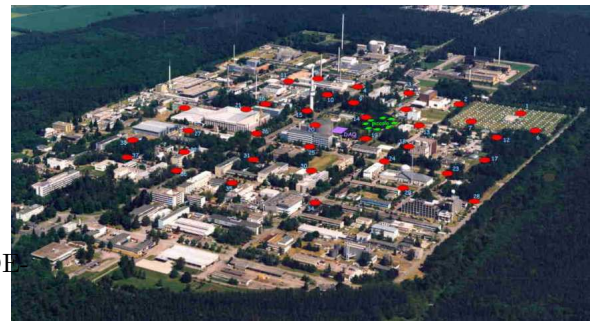

Figure 7: KASCADE-Grande array at Forschungszentrum Karlsruhe in Germany

One of the main results obtained by these two experiments is a picture of increasingly heavier composition above the knee caused by a break in the spectrum of the light components. Conventional acceleration models predict a change of the composition towards heavier components. The discovery of the knee in the heavy components, represented by iron, would be a convincing verification of these theories. From the observed rigidity dependent breaks of the spectra of different lighter primaries observed between 10^{14} and 10^{16} eV, the iron knee is expected around $E = 10^{17}$ eV.

A scintillator array measures the electrons, photons and muons outside the core region of extensive air showers in 252 detector stations on a rectangular grid of 13 m spacing, hence forming an array of $200 \times 200\,m^2$. The key component of the central detector is a finely segmented hadron calorimeter. Below 30 radiation length of absorber the central calorimeter contains a layer of 456 scintillation detectors acting as trigger for the calorimeter and measuring the arrival time of hadrons. A muon tracking detector is located north of the KASCADE-Grande central detector. The KASCADE-Grande detector array has been realized by means of 37 stations at a mutual distance of about 130 m covering an area of 0.5 km^2 next to the KASCADE site in order to operate jointly with the KASCADE detector components. Each KASCADE-Grande array station is equipped

with $10\,m^2$ of scintillation counters and electronic components to generate a trigger signal and for calibration purposes. A central data acquisition station (DAQ) collects the data from all stations and generates a valid experiment trigger. The KASCADE-piccolo trigger array consists of an array of 8 stations equipped with $10\,m^2$ of plastic scintillator each and is placed towards the center of the Grande array. The main aim of piccolo is to provide an external trigger to Grande and to KASCADE for coincidence events.

Pierre Auger Observatory [20]

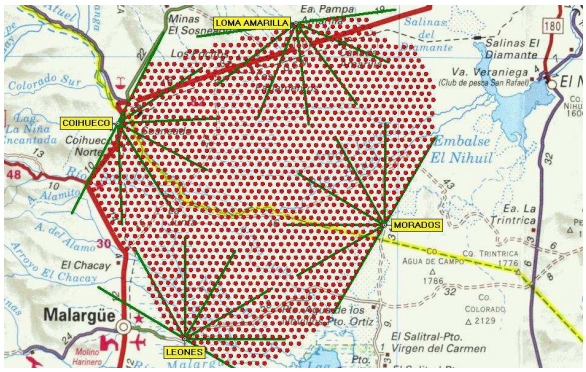

Figure 8: Pierre Auger Observatory array in the argentinean Pampa

The Auger Observatory is a "hybrid detector" employing two independent methods to detect and study high-energy cosmic rays up to an energy of 10^{20} eV.

The first ground-based detection method uses 1600 water tanks that cover an enormous section of the Pampa Amarilla (yellow prairie) in western Argentina and serve as particle detectors. Each 11400-litre tank, separated from each of its neighbours by 1.5 kilometres, contains photomultiplier tubes measuring the Cherenkov light produced by the incoming charged particles. The determination of the primary cosmic ray particle energy is based on the detected amount of light. Slight differences in the detection times at different tank positions permit to determine the trajectory of the incoming cosmic ray.

The observatory's second detection method uses optical detectors to observe the trail of nitrogen fluorescence and track the development of air showers by measuring the brightness of the emitted light. Using a grid of focusing mirrors to collect the light, cameras can view the air shower up to 15 kilometres away. While the fluorescence detectors only work on clear, moonless nights, the surface detectors are always operating regardless of atmospheric conditions.

The Auger Observatory is in the final stages of construction and has begun to collect data near Malargüe, Argentina. A matching site will also be built in southeastern Colorado, providing nearly uniform coverage of the skies in the northern and southern hemispheres. If cosmic rays are found to arrive from specific directions, the Auger Observatories will be able to identify and study possible cosmic ray sources all over the sky with equal sensitivity. If discrete sources are not found, the full-sky coverage provided by the two sites will be essential for determining whether cosmic-ray arrival directions are characterized by subtle large-scale patterns in the universe, or whether they are completely arbitrary.

2 Propagation of cosmic rays in the Earth's atmosphere

We have seen that cosmic rays interact with particles in the Earth's atmosphere and cause extensive air showers of high-energetic secondary particles, which are detectable by ground-based experiments. Direct detection of cosmic rays by balloon experiments is made in an altitude of 40 km, where the cosmic-ray particles traverse a matter grammage of $3 - 5\,\mathrm{g/cm^2}$. Even if these thickness is not enough to produce a full air shower, it produces supplementary secondary particles, which will be detected and measured and will cause thereby an additionally systematic error of the collected data. For an estimation of this systematic error it is necessary to know appropriately the structure and the composition of the Earth atmosphere and at least the fragmentation process of the nuclei.

2.1 Structure and composition of the Earth's atmosphere [21]

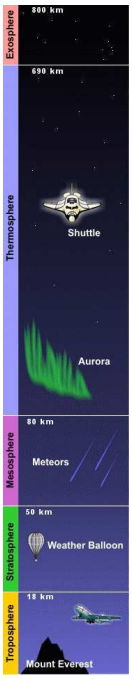

(a) Layers of the atmosphere leading to space [21]

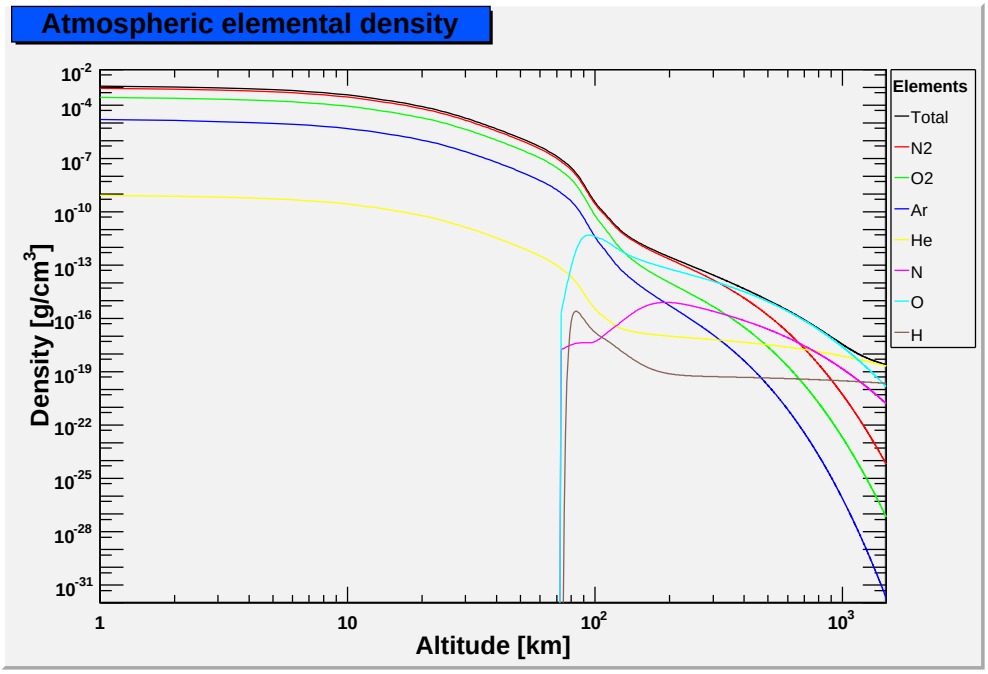

(b) Elemental density in the Earth's atmosphere as function of the altitude in km calculated by the NRLMSISE-00 model

Figure 9: Structure and composition of the Earth's atmosphere

The atmosphere may be conceptually divided into several layers, according to its thermal and ionisation structure. Each of the layers are bounded by "pauses" where the maximum changes in thermal characteristics, chemical composition, movement, and density occur. The troposphere, the first layer, begins at the Earth's surface and extends up to $6 - 20$ km high. As the gases in this layer decrease with height, the air become thinner and thereby the temperature also decreases. Above it, there is a layer in which temperature increases upward because of ozone absorption of solar radiation, the stratosphere. The stratosphere extends from the tropopause up to 50 km above the Earth's surface. This layer holds 19 percent of the atmosphere's gases. The scientific balloon experiments are flying in this layer. Above this, the effect of the warming by ultraviolet radiation becomes less and less and hence the temperature decreases in the mesosphere, which extends from the stratopause to about 85 km above the earth. In the layer above, the thermosphere, which extends from the mesopause to 690 km above the Earth, the extremely energetic radiation causes the temperature to increase with height out to the outer reaches of Earth's atmosphere, the exosphere, where atoms and molecules escape into space and satellites orbit the Earth. Within the mesosphere and thermosphere, solar radiation is sufficiently energetic to ionise gases. This produces the ionosphere.

The Earth's atmosphere is basically composed of nitrogen (N_2, 78.084%), oxygen (O_2, 20.946%) and argon (Ar, 0.934%). In higher altitudes (> 75 km) we can also find helium (He), nitrogen (N), oxygen (O) and

hydrogen (H) atoms. So we know approximately the composition of the Earth's atmosphere, but for experiments as CREAM and AMS (for trapped particles) it is very important to know the concentration evolution of the atmospheric gases from the ground up to the upper atmosphere limits. For such analyses some models exists of which we have chosen the NRLMSISE-00 (see reference [22]).

> The NRLMSISE-00 empirical atmosphere model was developed by Mike Picone, Alan Hedin, and Doug Drob based on the MSISE90 model. The MSISE90 model describes the neutral temperature and densities in Earth's atmosphere from ground to thermospheric heights. Below 72.5 km the model is primarily based on the MAP Handbook tabulation of zonal average temperature and pressure. Below 20 km these data were supplemented with averages from the National Meteorological Center (NMC). In addition, pitot tube, falling sphere, and grenade sounder rocket measurements from 1947 to 1972 were taken into consideration. Above 72.5 km MSISE-90 is essentially a revised MSIS-86 model taking into account data derived from space shuttle flights and newer incoherent scatter results.

(quoted from http://modelweb.gsfc.nasa.gov/atmos/nrlmsise00.html)

This model gives for a given date (time (UT), day, year), a given geographical point (geographical latitude and longitude) and a given altitude the atmospheric gas densities. Figure 9(b) indicates the elemental density evolution of the different species present in the atmosphere as function of the altitude. Because the number of secondary particles produced in the atmosphere is directly connected to the traversed matter thickness, we represent in figure 2.1 the correlation between the grammage and altitude via the integral of the total density over a given altitude to infinity:

$$X(h) = \int_h^\infty \rho_{\text{tot}}(x)\,\mathrm{d}x \tag{24}$$

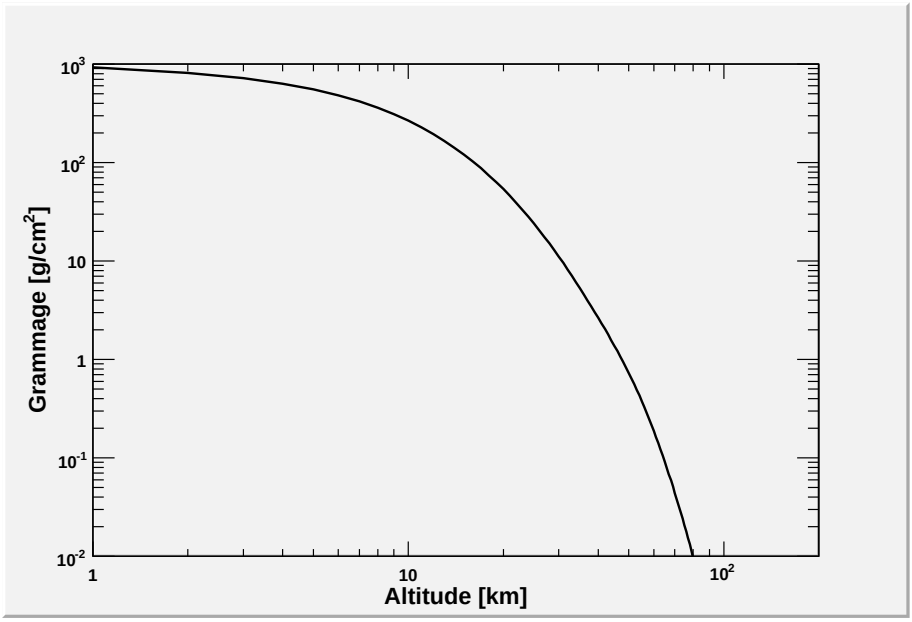

Figure 10: Correlation between grammage and altitude via the integral of the total density calculated by the NRLMSISE-00 model

We can see that the total thickness of the Earth's atmosphere is approximately $10^3\,\mathrm{g/cm^2}$, whereas the matter traversed for the particles measured by balloon experiments is only about $5\,\mathrm{g/cm^2}$. In comparison it may seem not a lot, but it is sufficient for the supplementary secondary production by the fragmentation processes with the atmospheric nuclei.

2.2 Fragmentation process

When cosmic rays interact with the interstellar medium, which is composed of 90% hydrogen and 10% helium, the main reaction is the spallation of the cosmic-ray particles. Hence, the isotopic composition of the primary cosmic ray flux changes. Basically one or two nucleons participate in nuclear interactions with high-energy

particles, but they are generally removed from the nucleus leaving it in a highly excited state. Several nuclear fragments evaporate from the nucleus. These are called spallation fragments, which are emitted more or less isotropically in the nuclei frame of reference. Additionally neutrons may be released from the spallation fragments, which could be fatal for light nuclei, regarding the possible imbalance between the numbers of neutrons and protons. When high energy nuclei undergo collisions with other heavy nuclei, the incident nucleuses leaves with a stream of relativistic spallation fragments, protons and neutrons [2].

The fragmentation processes in the Earth's atmosphere take place in the upper atmosphere and produces showers and spallation products of high energy. The projectile nucleus interacts with the most common atmospheric nuclei, the target nuclei, and produces some spallation fragments:

$$N_P + (N,\ O,\ Ar) \Longrightarrow \sum_F N_F \qquad \Longleftrightarrow \qquad \sigma_{PT}^F$$

For modelling and analysis of cosmic-ray data, the ability to calculate fragmentation cross sections with precision, because some of these cross sections could be measured but most other have to be calculated, becomes essential. Basic phenomenological models of the propagation of cosmic rays invariably make the simplifying assumption that cosmic-ray spallation products retain the same energy per nucleon as their progenitors. This is the so called straight-ahead approximation, which is a simplification and hence more practical from a computational point of view and justifiable at high energies ($> 2\,\mathrm{GeV/n}$).

2.3 Transport equation

We want to study the propagation of cosmic rays in the Earth's atmosphere at high energies. For this the straight-ahead approximation is valid and justified. We have seen in section 1.3.5 that the cosmic-ray flux, when it has traversed a matter slab of a given thickness x could be expressed in form of equation (10) at a given energy E_k:

$$\frac{\mathrm{d}N_i(x,E_k)}{\mathrm{d}x} = -\frac{1}{m_T}\sigma_{iT}(E_k)N_i(x,E_k) + \frac{1}{m_T}\sum_{j>i}\sigma_{iT}^j N_j(x,E_k), \tag{25}$$

where N_i are the abundances of the nucleus i at a depth x, m_T the target mass, σ_i the inelastic total cross section and σ_i^j the inelastic spallation cross section from a heavier nucleus j with the abundance N_j at a depth x to a nucleus i. The initial condition $N_i(0)$ taken here is the TOA flux abundance of a cosmic ray particle of charge Z, using equation (17) with the normalisation values given for the charges $Z = 1 - 28$ in table 1 and with the solar modulation given by equation (15).

We have also seen that in the Earth's atmosphere the number of targets to be considered is greater than one, due to the different atmospheric components. Hence we have to consider in equation (25) a sum over the different possible targets:

$$\frac{\mathrm{d}N_i(x,E_k)}{\mathrm{d}x} = \sum_T \frac{1}{m_T}\left(-\sigma_{iT}(E_k)R_T(x,E_k)N_i(x,E_k) + \sum_{j>i}\sigma_{iT}^j R_T(x,E_k)N_j(x,E_k)\right), \tag{26}$$

where $R_T(x) = \frac{\rho_T(x)}{\rho_{\mathrm{tot}}(x)}$ is the proportionality factor for the target nucleus T. The proportionality factor changes not significantly for altitudes between the Earth's surface and 200 km for the three main constituents, as we can see in figure 9(b). The typically values here are $R_N = 0.78$, $R_O = 0.21$ and $R_{Ar} = 0.01$. The implementation of this equation by using the NRLMSISE-00 model is discussed in the sections 3.3 and 4.1.

3 Cross sections

For our study of cosmic-ray propagation in the Earth's atmosphere the knowledge of the various cross sections is of great importance. The relevant cross sections are the total and the partial inelastic cross sections, where the first type describes the disappearance rate of a given element by interaction and the second type characterises the transformation laws of a parent nuclei in a given quantity of lighter nuclei. The cross sections are energy-dependent and we can experimentally distinguish three states:

1. $E_k \lesssim \mathrm{GeV/n} \Longrightarrow$ strong energy dependence (minimum at $\sim 200\,\mathrm{MeV/n}$)
2. $\mathrm{GeV/n} \lesssim E_k \lesssim \mathrm{TeV/n} \Longrightarrow$ the cross sections are practically constant
3. $E_k \gtrsim \mathrm{TeV/n} \Longrightarrow$ the cross sections increase slightly with energy

The measurements of all possible nucleus-nucleus cross sections, especially the fragmentation cross sections, are hardly realisable. But they are necessary for the propagation calculations as we can see in equation (25). Therefore, the precise calculation by programs becomes indispensable for cosmic-ray physics. Three types of approaches exists, based on microscopic, semi-empirical, and empirical formulations. In this section we will discuss two of theses different approaches (empirical and semi-empirical) for calculating the two cross section types and also their accuracy.

3.1 Total inelastic cross sections

An important input in our study is the total inelastic cross section, called also the total reaction cross section σ_R, defined as the total σ_T minus the elastic σ_{el} cross sections for two colliding ions:

$$\sigma_R = \sigma_T - \sigma_{el} \tag{27}$$

In the most simple model, the reaction cross sections are assumed to be proportional to the geometrical area of the interacting nuclei (πR^2, where R is the sum of the interacting nuclei radii). Most of the empirical models approximate the total reaction cross section according to Bradt-Peters with

$$\sigma_R = \pi r_0^2 \left(A_P^{1/3} + A_T^{1/3} - b_0 \right)^2 , \tag{28}$$

where r_0 is an energy-independent effective radius, b_0 is either an energy-independent or energy-dependent overlap or transparency parameter, and A_P and A_T are the projectile and the target mass numbers, respectively. This form of parametrisation works nicely for higher energies. However, for lower energies, Coulomb interaction becomes important and modifies reaction cross sections significantly.

3.1.1 The empirical Webber formula [23]

Webber & al propose another energy-independent formula based on the Bradt-Peters formula, but they observed that the energy-independent overlap parameter b_0 depends on both, the mass number of the target A_T and on the projectile A_P:

$$\sigma_{PT} = \pi r_0^2 \left\{ A_P^{1/3} + A_T^{1/3} - \left[t_0 - t A_T - \left(b' A_P^{1/3} A_T^{1/3} \right) \right] \right\}^2 , \tag{29}$$

where the nuclear radius r_0 is taken to be 1.35 fm and the other parameters are approximated as $t_0 = 1.36$, $t = 0.018$, and $b' = 0.0065$.

Equation (29) provides a good fit to all data for carbon targets, but for hydrogen targets, the value of b' is required to increase in order to fit the high Z beam data, indicating a rapid increase in the overlap parameter of conversely a greater transparency in the nuclear reaction cross section.

3.1.2 The semi-empirical formula by Letaw & al [24]

In the year 1983 Letaw & al proposed a simple formula for proton-nucleus reactions. Their approach is based on an empirical fit to the existing data at this time. The high-energy formula is

$$\sigma_R^{HE} = 45 A^{0.7} \left[1 + 0.016 \sin\left(5.3 - 2.63 \ln A\right) \right] \quad [\mathrm{mb}], \tag{30}$$

and is energy-independent. At energies below 2 GeV/n the total inelastic cross section is not independent of energy:

$$\sigma_R(E_k) = \sigma_R^{HE} \left[1 - 0.62 \exp\left(-E_k/200\right) \sin\left(10.9 E_k^{-0.28}\right) \right] \quad [\mathrm{mb}]. \tag{31}$$

These formulae for the total inelastic cross section of protons on nuclei is valid for nuclei of charge 2 or greater. For helium the high-energy formula (30) is modified by a factor 0.8, the correction for energy dependence at low energies is given by equation (31), modified for beryllium by the multiplicative factor $1 + 0.75 \exp(-E/75)$, where E is in MeV. The authors estimate for formula (31) an error $< 2\%$ for $E > 1\,\mathrm{GeV}$ and $< 5\%$ for $300\,\mathrm{MeV} < E < 1\,\mathrm{GeV}$.

3.1.3 Universal parametrisation of Tripathi & al [25, 26]

Tripathi & al present an universal parametrisation of total reaction cross sections for any system of colliding nuclei that is valid for the entire energy range from a few MeV/n to a few GeV/n. The universal picture presented here treats proton-nucleus, neutron-nucleus and nucleus-nucleus collision. The authors start with a Bradt-Peters formulation (28), which works nicely for higher energies. However, for lower energies, Coulomb interaction becomes important and modifies reaction cross sections significantly. In addition, strong absorption models suggest an energy dependence of the interaction radius. For the neutron-nucleus collisions, there is no Coulomb interaction, but the total reaction cross section for these collisions is modified by the strength of the imaginary part of the optical potential at the surface, which was incorporated by introducing a low-energy multiplier X_m that accounts for the strength of the optical model interaction. Incorporating these effects they propose the following form for the reaction cross section:

$$\sigma_R = \pi r_0^2 \left(A_P^{1/3} + A_T^{1/3} + \delta_E \right)^2 \left(1 - R_c \frac{B}{E_{\mathrm{cm}}} \right) X_m, \tag{32}$$

where $r_0 = 1.1\,\mathrm{fm}$ and E_{cm} is the colliding system centre of mass energy in MeV/n. The second to last term on the right-hand side is the Coulomb interaction term which modifies the cross section at lower energies and becomes less important as the energy increases (typically after several tens of MeV/n). The Coulomb multiplier R_c is needed in order to have the same formalism for the absorption cross sections for light, medium, and heavy systems. B is the energy-dependent Coulomb interaction barrier, and is given by

$$B = \frac{1.44 Z_P Z_C}{R},$$

where Z_P and Z_T are atomic numbers of the projectile and target, respectively. R is the radius for evaluating the Coulomb barrier height, it is

$$R = r_P + r_T + \frac{1.2 \left(A_P^{1/3} + A_T^{1/3} \right)}{E_{\mathrm{cm}}^{1/3}},$$

where r_i is equivalent hard sphere radius and is related to the $r_{\mathrm{rms},i}$ radius by

$$r_i = 1.29 r_{\mathrm{rms},i},$$

with $i = P, T$.

Energy dependence in the reaction cross section at intermediate and higher energies is mainly because of two effects: transparency and Pauli blocking; this is taken into account in δ_E, which is

$$\delta_E = 1.85 S + \frac{0.16 S}{E_{\mathrm{cm}}^{1/3}} - C_E + \frac{0.91 (A_T - 2Z_T) Z_P}{A_T A_P},$$

where S is the mass asymmetry term, defined as

$$S = \frac{A_P^{1/3} A_T^{1/3}}{\left(A_P^{1/3} + A_T^{1/3} \right)}$$

and is related to the volume overlap of the collision system. The term C_E is related to the transparency and Pauli blocking and is given by

$$C_E = D \left[1 - \exp\left(-\frac{E}{T_1} \right) \right] - 0.292 \exp\left(-\frac{E}{792} \right) \cos\left(0.229 E^{0.453} \right),$$

where the collision kinetic energy E is in MeV/n. Here D is related to the density dependence of the colliding system and can be nicely related to the densities of the colliding systems for medium and heavier systems. This in effect simulates the modifications of the reaction cross sections due to Pauli blocking.

The optical model multiplier X_m is given by

$$X_m = 1 - X_1 \exp\left(-\frac{E}{X_1 S_L}\right)$$

with

$$X_1 = 2.83 - (3.1 \cdot 10^{-2}) A_T + (1.7 \cdot 10^{-4}) A_T^2.$$

The function S_L for light systems as used here is

$$S_L = 1.2 + 1.6 \left[1 - \exp\left(-\frac{E}{15}\right)\right].$$

The optical model multiplier is for all reactions of type p+A and A+A equal to 1.

3.2 Fragmentation cross sections

In contrary to the total inelastic cross sections the measurements of the fragmentation cross sections are not so easy to realise. In consequence, the available data is humble. By its astrophysical importance for the cosmic-ray studies, the multifragmentation constitutes a vast study domain. The precise calculation of the fragmentation cross sections becomes necessary and has different approaches. A lot of models based on a microscopic approach exist, but none of them is capable to reproduce the fragmentation cross sections satisfyingly. In the year 1990 the team around W. R. Webber published their results of the fragmentation study, which were completed in the following years and which represent around 500 individual elemental cross sections. They also proposed an empirical formula calculating the fragmentation cross section for a given element, which is discussed in this section. The precursor of the common model of Webber is the semi-empirical formulation of fragmentation cross sections proposed by R. Silberberg and C. H. Tsao in the 70th.

3.2.1 Semi-empirical formula by Silberberg and Tsao [27, 28]

The fragmentation cross sections have some properties which permit a semi-empirical formulation. This properties are principally connected to the mass difference $\Delta A = A_T - A_F$ between the target and the fragment nucleus and to the ratio of the neutron-to-proton number of the fragment nucleus. Silberberg and Tsao propose a semi-empirical equation for proton-nucleus interactions:

$$\sigma^p(Z_i, A_i, Z_F, A_F, E_i) = \sigma_0 f(A_F) f(E_i) \exp\left(-P\Delta A\right) \exp\left(-R\left|Z_F - SA_F + TA_F^2\right|^\nu\right) \Omega\eta\xi, \tag{33}$$

where σ_0 is a normalisation factor and $f(A_F)$ and $f(E_i)$ are correction factors applicable to products from heavy targets with $Z_T > 30$. The factor $\exp\left(-P\Delta A\right)$ describes the diminution of cross sections as the difference of target and product mass ΔA increases, where P is the target mass dependence. The factor $\exp\left(-R\left|Z_F - SA_F + TA_F^2\right|^\nu\right)$, where the exponent ν is taken to be 3/2, describes the distributions of cross sections for the production of various isotopes of an element of atomic number Z_F. The width of the distribution is represented by the parameter R. The parameter S describes the location of the peaks of theses distribution curves and the parameter T describes the shift of the distribution curves toward greater neutron excess as the atomic number of the product increases. The factors Ω, η and ξ are the nuclear structure factor, the nucleon pairing factor and the enhancement factor for light evaporation products, respectively. At last, E_i is the kinetic energy of the projectile in MeV.

The enlargement of the model for nucleus-nucleus reactions is made by a scaling of the proton-nucleus partial cross sections σ^p. This scaling is done by a scaling parameter S_c, which is based on a Bradt-Peters-type law, and additional enhancement factors:

$$\sigma(Z_P, A_P, Z_F, A_F, E_P) = S_c \epsilon_L \epsilon_\Delta \epsilon_1 \sigma^p(Z_P, A_P, p, E_p), \tag{34}$$

where $\sigma^p(Z_P, A_P, p, E_p)$ is the partial cross section of proton-nucleus reactions given by equation (33) for breakup of nuclides (A_P, Z_P) colliding with protons (E_p), ϵ_L is the enhancement factor for the lightest products Li, Be and B, ϵ_Δ is the enhancement factor for reactions with a large value of ΔA and ϵ_1 is the enhancement factor for single-nucleon stripping, caused by the giant dipole resonance.

3.2.2 Empirical formula by Webber & al [29]

Webber & al proposed in 1990 a new empirical formula for calculating the partial cross sections for the production of secondary fragments with energy $E \gtrsim 200\,\mathrm{Mev/n}$ in hydrogen targets. This formula and the systematics of these cross sections are based on their fragmentation study, which has resulted more than 100 secondary elemental cross sections and over 300 secondary isotopic cross sections. The cross section formula is a product of three essentially independent terms:

$$\sigma(Z_P, A_P, Z_F, A_F, E) = \sigma_0(Z_F, Z_P) f_1(Z_F, A_F, Z_P, A_P) f_2(E, Z_F, Z_P). \tag{35}$$

The total cross section σ for a particular final charge Z_F, mass A_F and energy E depends on

1. the charge changing cross section $\sigma_0(Z_F, Z_P)$:

$$\sigma_0(Z_F, Z_P) = \sigma_{Z_F} \exp\left(\frac{-(Z_P - Z_F)}{\Delta_{Z_F}}\right) \exp\left(\frac{-|N_{Z_P} - N_{0Z_F}|}{8.5}\right). \tag{36}$$

   σ_{Z_F} and Δ_{Z_F} are fitting parameters. The first exponential term represents the fact that the elemental cross sections into particular Z_F can be well represented by an exponential function of the difference $Z_P - Z_F$ for any Z_i. The second exponential term is related to the observation that the production of a secondary nucleus is a maximum when the primary and secondary nucleus both have A_P and A_F near the mass stability line. $N = A - 2Z$ is the neutron excess, where N_0 defines the line of β stability.

2. the isotopic cross section distribution term $f_1(Z_F, A_F, Z_P, A_P)$:

$$f_1(Z_F, A_F, Z_P, A_P) = \frac{1}{\delta_{Z_F}\sqrt{2\pi}} \exp\left(\frac{-(N - N_{Z_F})^2}{2\delta_{Z_F}}\right). \tag{37}$$

   Here N_{Z_F} is the neutron excess of the centroid of the mass distributions of the cross sections for each charge and δ_{Z_F} is the characteristic width of these mass distributions.

3. the energy dependence term $f_2(E, Z_F, Z_P)$:

$$\begin{aligned} f_2(E, Z_F, Z_P) \;=\; & 1 + m(\Delta Z)\left(\frac{Z_P}{26}\right)^{2.5} \exp\left(\frac{-(E - E_m)^2}{\Delta E_m}\right) \\ & + n(\Delta Z)\left(\frac{Z_P}{26}\right)^{1.4} \exp\left(\frac{-(E - E_n)^2}{\Delta E_n}\right) \\ & + o(\Delta Z)\left(\frac{Z_P}{26}\right)^{0.4} \exp\left(\frac{-(E - E_o)^2}{\Delta E_o}\right) \\ & + p(\Delta Z)\frac{Z_P}{26} \exp\left(\frac{-(E - 2000)}{2000}\right). \end{aligned} \tag{38}$$

   Each of these four terms of the sum describes a behaviour for a given energy until reaching the asymptotic limit above some GeV/n. The values of $m(\Delta Z)$, $n(\Delta Z)$, $o(\Delta Z)$, $E_{m,n,o}$ and $\Delta E_{m,n,o}$ are derived from fitting the data.

In addition to these three basic terms, there are specialized terms for neutron and proton stripping reactions.

Additionally Ferrando & al propose an empirical formula for the measured σ_{He}/σ_p ratios, allowing to include the set of α-particle reactions in propagation calculations [30]:

$$\frac{\sigma_{He}}{\sigma_p}(Z_P, Z_F, E) = \exp\left[\mu(E)|(Z_P - Z_F) - f(Z_P)\delta_{Fe}(E)|^{1.43}\right], \tag{39}$$

where $\mu(E)$, $\delta_{Fe}(E)$ are linearly interpolated as a function of energy from those used for Fe, and $f(Z_P)$ linearly interpolated as a function of Z_P from values for three Z_P.

This model has not been extended to nucleus-nucleus reactions and calculates only spallation cross sections on hydrogen and helium. Seen its precision, which lies for the fragmentation cross sections between 5 and 10% and which is smaller in comparison to the Silberberg and Tsao model (they estimate an error $\sim 35\%$), we will use the Webber code for the cross section calculations. For calculating the cross sections for nucleus-nucleus reactions we need a multiplicative factor, comparable to the scaling factor in the Silberberg and Tsao formula, justified by the factorisation of cross sections.

3.2.3 Factorisation

The above discussed models for fragmentation cross section calculations are primarily considered for cosmic-ray propagation in the interstellar medium. That means that the models gist is the estimation of the fragmentation cross sections on hydrogen and helium targets. For our study of the elemental cosmic-ray propagation in the Earth's atmosphere, constituted basically of nitrogen and oxygen, we need the fragmentation cross sections σ^F_{PT} for nucleus-nucleus reactions, which we can estimate with the help of a scaling factor, described below.

The concept of the factorisation of fragmentation cross sections originated in the description of processes in high-energy physics during the 70th. The concepts of "strong" and "weak" factorisation have been developed, which at high enough beam energies can be expressed as:

$$\sigma^F_{PT} = \gamma^F_P \gamma_T \qquad \text{for strong factorisation and} \tag{40}$$

$$\sigma^F_{PT} = \gamma^F_P \gamma_{PT} \qquad \text{for weak factorisation,} \tag{41}$$

where σ^F_{PT} is the nuclear fragmentation cross section for the projectile P incident upon the target T producing the fragment F, γ^F_P is a factor which depends only upon the species of projectile and fragment, γ_{PT} is a factor which depends only on the species of projectile and target, and γ_T is a factor which is a function solely of the target species.

We are looking for a scaling factor γ_S, which scales the proton-nucleus cross sections to nucleus-nucleus cross sections

$$\sigma^F_{PT} = \gamma_S \cdot \sigma^F_{P\,H} \tag{42}$$

and which is based on a Bradt-Peters formulation and also takes advantage of the weak-factorisation property of projectile fragments. The following relation was found to describe γ_{PT} [31]:

$$\gamma_{PT} = g\left(A_P^{1/3} + A_T^{1/3} - b(A_P, A_T)\right), \tag{43}$$

where g, the geometrical factor, and b, the overlap parameter, are free parameters.

Scaling to proton-nucleus cross sections in our procedure essentially means

$$\gamma_S \qquad \Longrightarrow \qquad \gamma_{PT}.$$

Semi-empirical expressions for g and $b(A_P, A_T)$ can be written as:

$$g = \frac{\sigma^F_{P\,He}}{\sigma^F_{P\,H}} \frac{1}{(A_P^{1/3} + 1 - b(A_P, H))} \tag{44}$$

$$b(A_P, A_T) = 1.36 - 0.018 \cdot A_T - 0.065 \cdot A_P^{1/3} A_T^{1/3}, \tag{45}$$

where our geometrical factor g is normalized to the ratio of the fragmentation cross section for a helium target to this for a hydrogen target. For the overlap parameter b we are using the proposed form given by the Webber formulation in equation (29) of the total inelastic cross section [23].

3.3 Implementation with the USINE software

The first problem that occurs to us was that the programs calculating the fragmentation cross sections, which we need for the implementation of the transport equation (25) for the propagation of cosmic rays in the Earth's atmosphere, are no more accessible. Because the programming of the different formulae, discussed in the sections above, would take too much time, we searched for people, who are using the various programs.

We got the unlimited support of David Maurin, which made the work, described here in this thesis, possible. David Maurin used the software of Webber & al and implemented the cross section formula of Tripathi & al [32]. In his kindness he placed at our disposal his propagation software USINE, which he developed in C++ with the contributions of R. Taillet, P. Salati, F. Donato and C. Combet. This software deals with propagation of galactic ray cosmic ray nuclei (all existing nuclei) and antinuclei (antiprotons and antideuterons) in various propagation models (leaky box model, diffusion model...).

The USINE package contains basic tools to describe cosmic ray nuclei, like the cross section data from different codes and solar modulation models, which we use for the implementation of the transport equation with solar modulated fluxes.

The considered energy range is implemented by using an USINE class, which defines a vector of the user-defined quantity, containing the quantity values, with a given unity and a given number of steps, which could

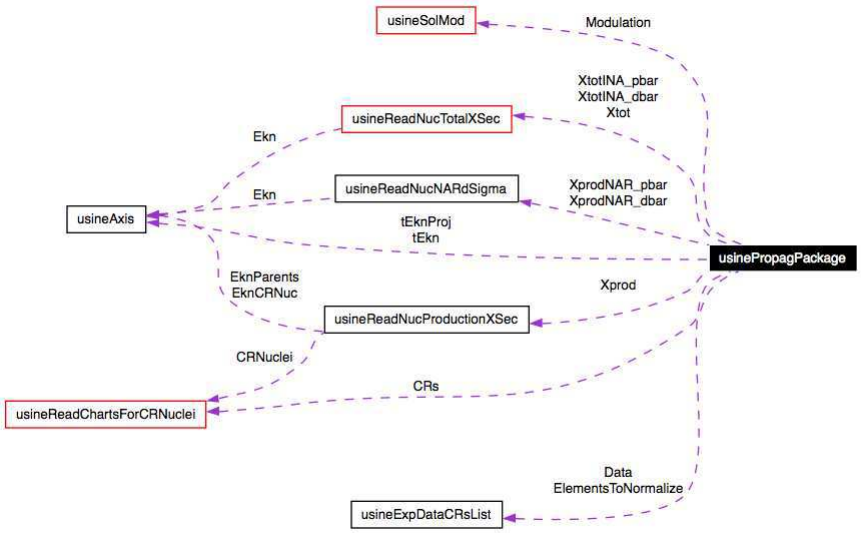

Figure 11: Structure of the USINE Propagation package [32].

either be linear or logarithmic. In our case a logarithmic energy axis in GeV/n from a minimum to a maximum energy value with a number of steps, which are all input parameters of the program, is defined.

The nuclear data of all nuclei (^{1}H to ^{70}Zn) are contained in a data file, which is used to create a list of cosmic-ray nuclei that we want to propagate. From this nuclei list another list, containing the "parent" nuclei, could be generated. But only nuclei whose halflife is of the order of the propagation time are considered. The principle used is the so called cascade method, which says, that the heaviest nucleus of the cosmic ray list does not have a parent, a heavier nucleus, which could produce it via fragmentation. The second heaviest nuclei can only have the heaviest nuclei as parent and so on. That means that the lightest nucleus has all heavier nuclei as parents. These list can be easily handled.

Additionally the information of the interstellar cosmic-ray fluxes given in table 1 are stored in a data file, which can be used for the implementation of the elemental cosmic-ray fluxes through the equation (17). A class of the USINE code permits to transform the interstellar fluxes into TOA fluxes via various methods (force field or spherical symmetry method).

The total inelastic cross sections are calculated by a function using the formulation of Tripathi & al (see section 3.1.3), Sihver & al, or Wellish & al. We are using the Tripathi & al formulation, because this gives the most precise results. The fragmentation cross sections are also stored in data files, which resulted from the different programs (Webber & al or Tsao & Silberberg, see sections 3.2.2 and 3.2.1). A function calls the chosen data file.

Indeed we got the entire USINE code, but we just use some classes for the implementation of

- a logarithmic energy grid,
- a cosmic ray nuclei list and the corresponding parent nuclei list,
- the total inelastic and the fragmentation cross sections,
- the interstellar cosmic ray fluxes and
- their solar modulation with the force field approximation.

We want to present an example of the cross sections calculated with the USINE software for the two cosmic ray nuclei ^{11}B and ^{12}C in figure 12. For the total inelastic cross sections the universal parametrisation of Tripathi & al was used. The resulting cross sections on ^{14}N, ^{16}O and ^{40}Ar targets are shown in figure 12(a). We can see the characteristic shape with the strong energy dependence for small energies, the minimum around 200 MeV/n and the energy independence above 2 GeV/n. The fragmentation cross sections of the ^{12}C nucleus into the ^{11}B nucleus on the above listed target nuclei is calculated with the help of the Webber & al formulation. The represented lines on figure 12(b) are energy independent above an energy of 4 GeV/n.

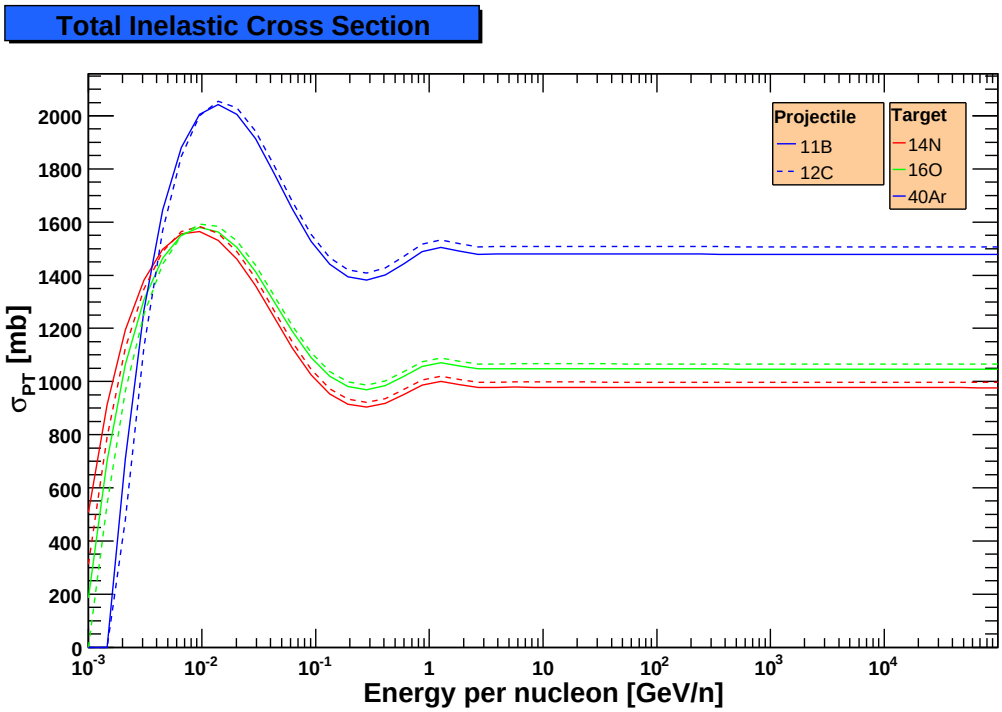

(a) Total inelastic cross sections of ^{11}B and ^{12}C on ^{14}N, ^{16}O and ^{40}Ar calculated by the Tripathi & al formulation using the USINE software

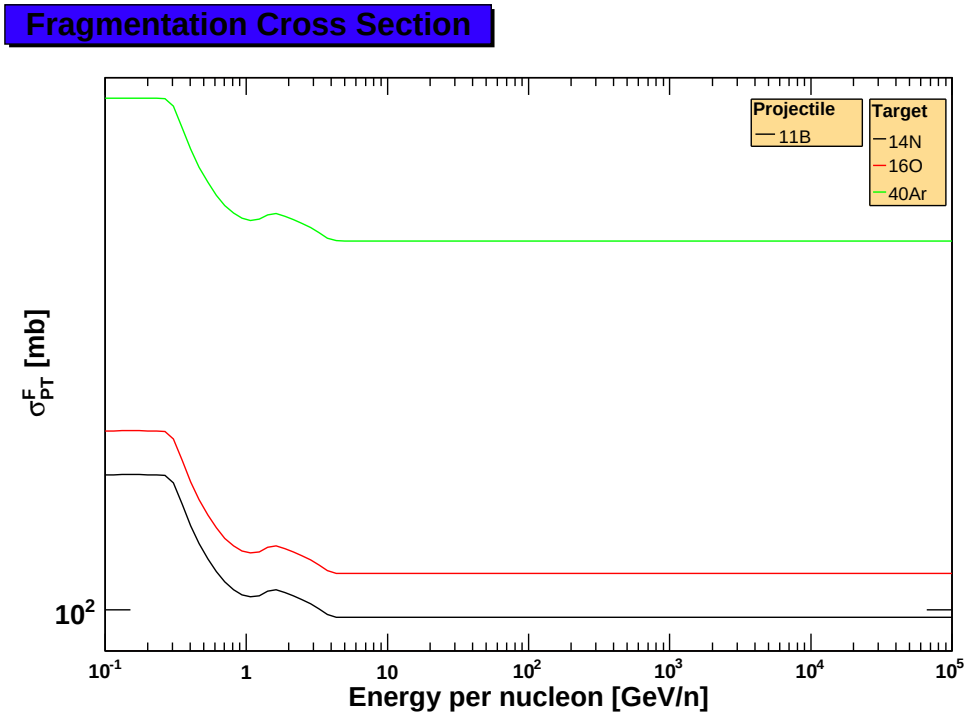

(b) Fragmentation cross sections of ^{11}B on ^{14}N, ^{16}O and ^{40}Ar calculated by the Webber & al formulation using the USINE software

Figure 12: Implementation of the total inelastic and fragmentation cross sections with the USINE software of David Maurin.

4 Study of the fragmentation process in the Earth's atmosphere

The propagation of cosmic rays in the Galaxy is until now not very well understood. A lot of propagation models have been developed, of which two are very common used: the Leaky Box model and the diffusion model. The secondary-to-primary ratios of cosmic rays are physically from great interest, because they are a good test for the different propagation models. Especially the boron-to-carbon (B/C) ratio has always been considered the best quantity to study diffusion properties. For example, diffusive reacceleration contributes significantly in shaping the B/C ratio at kinetic energy per nucleon around 1 GeV/n. It can naturally explain the observed bump at this energy, without invoking any artificial break in the diffusion coefficient. At high energies, i.e. $10\,\mathrm{GeV/n} \leq E_k \leq 10^5\,\mathrm{GeV/n}$, the parameter which mostly shapes the B/C ratio is the diffusion coefficient slope or the so called spectral index δ.

Experiments, which are looking for the secondary-to-primary ratios like AMS and CREAM are biased by the supplementary production of secondary particles, and by the absorption of primary and secondary particles during the traverse of the Earth's atmosphere and the detector. It is therefore important to take these effects into account in the data analysis.

4.1 Implementation of the transport equation

The first approach to solve the transport equation (26) was to directly integrate the diffusion equation at each energy E_k:

$$N_i(x+\Delta x, E_k) = N_i(x, E_k) + \Delta x \left[\sum_T \frac{R_T(x)}{m_T} \left(-\sigma_{iT}(E_k) N_i(x, E_k) + \sum_{j>i} \sigma_{iT}^j(E_k) N_j(x, E_k) \right) \right], \tag{46}$$

with $N_i(0, E_k) = \phi_i^{\mathrm{mod}}(E_k)$ the TOA flux of the particle of the type i at the energy E_k. The numeric integration was made by an iterative method from a grammage of $0\,\mathrm{g/cm^2}$ to a grammage $x\,\mathrm{g/cm^2}$, by using a step Δx, which are both program input parameters.

The considered energy range, cosmic ray nuclei and parent nuclei list, the TOA fluxes and the cross sections are implemented by using the method described in section 3.3. The fragmentation cross sections used here are on hydrogen and helium targets, so we need to scale these with the scaling factor γ_S given by the equations (43) and (44) to obtain the fragmentation cross sections for nucleus-nucleus reactions.

The disadvantage of the method of numeric integration is, that for the data analysis, where we get the propagated cosmic-ray fluxes, and we want to extract the interstellar fluxes, the reverse process is more complicated and costs also a lot of time. Therefore we focused on a matrix formulation of the problem, because the matrix can easily be inverted for the data analysis.

The solution of the transport equation (26) can be expressed as follows:

$$\tilde{N}(x, E_k) = \exp\left(S(x, E_k)\right) \tilde{N}(0, E_k), \tag{47}$$

where $\tilde{N}(0, E_k)$ is the vector containing all the abundances of the considered cosmic-ray nuclei at the top of the atmosphere, the vector $\tilde{N}(x, E_k)$ is the resulting vector containing the abundances of the considered cosmic ray nuclei at a grammage of $x\,\mathrm{g/cm^2}$. In the following the energy per nucleon dependence will be omitted in the notations. $R(x) = \exp\left(S(x)\right)$ is the response matrix and S is the upper triangular transformation matrix, where the diagonal elements correspond to the absorption and the other elements to the production of the cosmic-ray nuclei:

$$S(x) = \sum_T \int_0^x \frac{R_T(x')}{m_T} \mathrm{d}x' \begin{pmatrix} -\sigma_{1T} & \sigma_{2T}^1 & \cdots & \sigma_{nT}^1 \\ 0 & -\sigma_{2T} & \cdots & \sigma_{nT}^2 \\ & & \ddots & \vdots \\ 0 & 0 & 0 & -\sigma_{nT} \end{pmatrix} \tag{48}$$

Now to calculate the exponential of the matrix $S(x)$ we can make the approximation:

$$\begin{aligned} R(x) &= \exp\left(S(x)\right) \\ &= \left(\mathbb{1} + \frac{S(x)}{n}\right)^n, \end{aligned}$$

which is exact for $n \to \infty$. The value of n is chosen in order to get the needed accuracy. That gives us finally:

$$\tilde{N}(x) = \left(\mathbb{1} + \frac{S(x)}{n}\right)^n \tilde{N}(0) \tag{49}$$

For calculating the matrix multiplication, the "TMatrix" library of the ROOT environment is used.

In figure 13(a) an example of non-propagated and propagated cosmic ray fluxes for a spectral index $\delta = 0.3$ is represented, where we implemented a cosmic ray nuclei list containing the two nuclei ^{11}B and ^{12}C. We can see the TOA fluxes (depth $= 0\,\mathrm{g/cm^2}$) of ^{11}B (black line) and ^{12}C (red line) and the propagated fluxes of ^{11}B (black dashed line) and ^{12}C (red dashed line) at a grammage of $5\,\mathrm{g/cm^2}$ of the Earth's atmosphere. The propagated flux of ^{12}C is parallel to the TOA flux, because ^{12}C has as the heaviest nucleus no parents in the cosmic ray nuclei list. In contrary the propagated flux of ^{11}B surmount the TOA flux as a consequence that the production through the parental nucleus ^{12}C becomes dominant at high energies.

In a second step, the propagation of the B/C ratio for various spectral indices δ are studied. In the paper of A. Castellina and F. Donato [33], where they study the B/C ratios for different δ with the help of an older version of the USINE software [32], figure 1 on page 152 represents the B/C ratios as a function of kinetic energy per nucleon with five theoretical predictions corresponding to $\delta = 0.3$, 0.46, 0.6, 0.7, 0.85. These five curves are represented in figure 13(b) (continuous lines). We can see that for small energies the predictions for B/C ratio in the $\delta = 0.3$ and $\delta = 0.85$ are close. But for an energy of $\sim 10\,\mathrm{TeV/n}$ these two cases differ by more than one order of magnitude. We see here that after a travel of the cosmic ray nuclei through $5\,\mathrm{g/cm^2}$ of the Earth's atmosphere, the B/C ratios (dashed lines in the figure 13(b)) becomes at high energy practically constant, due to the effect, that the production of ^{11}B by the heavier nucleus ^{12}C in the Earth's atmosphere becomes dominant.

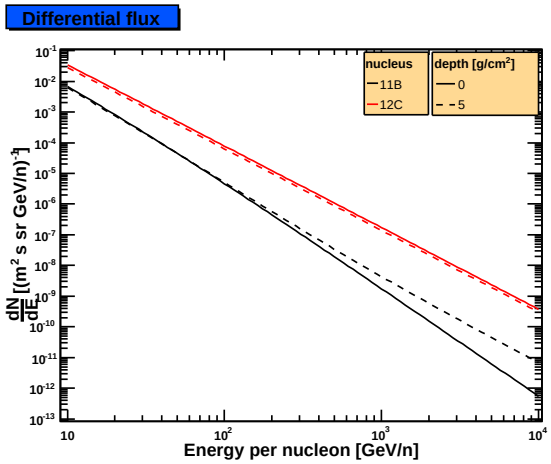

(a) Differential fluxes with an spectral index $\delta = 0.3$ as a function of the kinetic energy per nucleon at the top of the atmosphere (continuous lines) and at a traversed matter thickness of 5 g/cm^2 (dashed lines) of the cosmic ray nuclei ^{11}B (black lines) and ^{12}C (red lines)

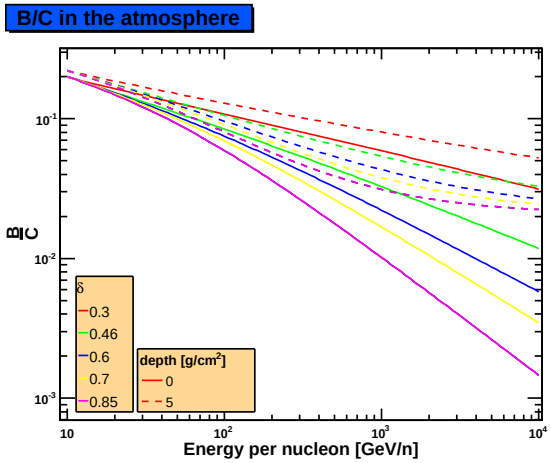

(b) Boron-to-carbon (B/C) ratios as a function of the kinetic energy per nucleon at the top of the atmosphere (continuous lines) and at a traversed matter thickness of 5 g/cm^2 (dashed lines) for 5 different spectral indices δ (0.3, 0.46, 0.6, 0.7, 0.85)

Figure 13: Results of the transport equation implementation

In the same figure 13(b) we can recognise the importance of the cosmic-ray propagation study in the Earth's atmosphere. After a traverse of only $5\,\mathrm{g\,cm^{-2}}$ of the Earth's atmosphere the B/C ratio for all δ changes significantly, especially for the case of $\delta = 0.85$, where the B/C ratios differ by more than one order of magnitude. Therefore, it is necessary to correct this phenomenon during the reconstruction of the TOA fluxes in the data analysis.

In conclusion, the matrix method is easy to handle for the propagation calculation and for the data analysis by inverting it. Additionally we have seen that the production of secondary particles in the Earth's atmosphere is important and biases significantly the measured secondary-to-primary ratios. Hence, the measurements have to be corrected during the data analysis.

4.2 Unfolding test

The reconstruction of the TOA fluxes from the data is based on inverting the transformation matrix $R(x)$. The inversion of the matrix for the data analysis may produce distortions to the extracted distributions, which may occur because the values of the cosmic-ray fluxes are subject to additional random fluctuations. This distortions are due to the fact, that the number of measured particles $\tilde{n}(x)$, which are random variables and hence subject to statistical error, is not equal to the expected number of particles $\tilde{\mu}(x)$. The procedure of correcting for these distortions is known as unfolding [34]. This is strictly equivalent to the deconvolution of measured spectra from the detector response.

To test if we have or not an unfolding problem, we need to compare at each energy E_k the simulated TOA fluxes, reconstructed from the fluxes measured in the Earth's atmosphere and which have suffered some statistical fluctuations, with the expected TOA fluxes of all considered nuclei. Therefore the following procedure was made for each energy E_k in a given energy range:

1. The vector $\tilde{N}(0)$ containing the TOA fluxes of the considered cosmic-ray nuclei for a given energy E_k was created:
$$\tilde{N}(0) = \begin{pmatrix} N_1(0) \\ N_2(0) \\ \vdots \\ N_n(0) \end{pmatrix} \tag{50}$$
These TOA fluxes are represented on the right hand side plot in figure 14 by the solid lines.

2. With the help of the response matrix $R(x)$ these TOA fluxes were propagated till the given grammage $x\,\mathrm{g/cm^2}$of the Earth's atmosphere:
$$\tilde{N}(x) = R(x)\tilde{N}(0). \tag{51}$$
The solid lines in the left hand side plot on figure 14 represent here the propagated fluxes for $x = 5\,\mathrm{g/cm^2}$.

3. Now the expectation values of the particle number $\tilde{\mu}(x)$, measured by a detector with an acceptance A between the energy E_k and $E_k + \Delta E_k$, for a measurement time T can be calculated by the equation:
$$\tilde{\mu}(x) = AT\Delta E_k \tilde{N}(x). \tag{52}$$
The acceptance A was taken to be $1\,\mathrm{m^2\,sr}$ and the measure time $T = 100\,\mathrm{days}$.

4. We simulated then the particle number (vector $\tilde{n}(x)$) for the given energy bin ΔE_k, detected by the above considered detector. We assumed here that the detected particles $n_i(x)$ follows a Poisson distribution law centred on the expectation value $\mu_i(x)$:
$$P(n_i(x) = k) = \frac{\mu_i(x)^k}{k!}\mathrm{e}^{-\mu_i(x)}, \tag{53}$$
where k is an integer.

5. With these vector of reconstructed particle numbers for each cosmic ray nucleus, the simulated cosmic ray fluxes $\tilde{\phi}(x)$ for the energy E_k are given by:
$$\tilde{\phi}(x) = \frac{\tilde{n}(x)}{AT\Delta E_k}. \tag{54}$$
These reconstructed fluxes of the simulation are represented on the left hand side plot on the figure 14 by the histograms. We can see the statistical fluctuations, which become more important for high-energy bins.

6. The last step is the reconstruction of the TOA cosmic-ray flux from the simulated fluxes $\tilde{\phi}(x)$ at the energy E_k. The vector $\tilde{\phi}(0)$ is calculated with the help of the inverted response matrix $R^{-1}(x)$:
$$\tilde{\phi}(0) = R^{-1}(x)\tilde{\phi}(x). \tag{55}$$
At this step we can see if an unfolding problem exists. The different reconstructed TOA fluxes $\phi_i(0)$ of the simulation are represented by the histograms on the right hand side plot in figure 14.

We can see that the reconstructed TOA fluxes of the simulation $\tilde{\phi}(0)$ for the considered cosmic-ray nuclei correspond over the whole energy range to the initial cosmic-ray flux $\tilde{N}(0)$, even the "zero" flux apart from some statistical fluctuations for the cosmic-ray nucleus ^{13}C is obtained. Consequently we do not have an unfolding problem by inverting the response matrix $R(x)$. This could be explained by the fact, that the eigenvalues of the response matrix $R(x)$ are close to one for the given depth x.

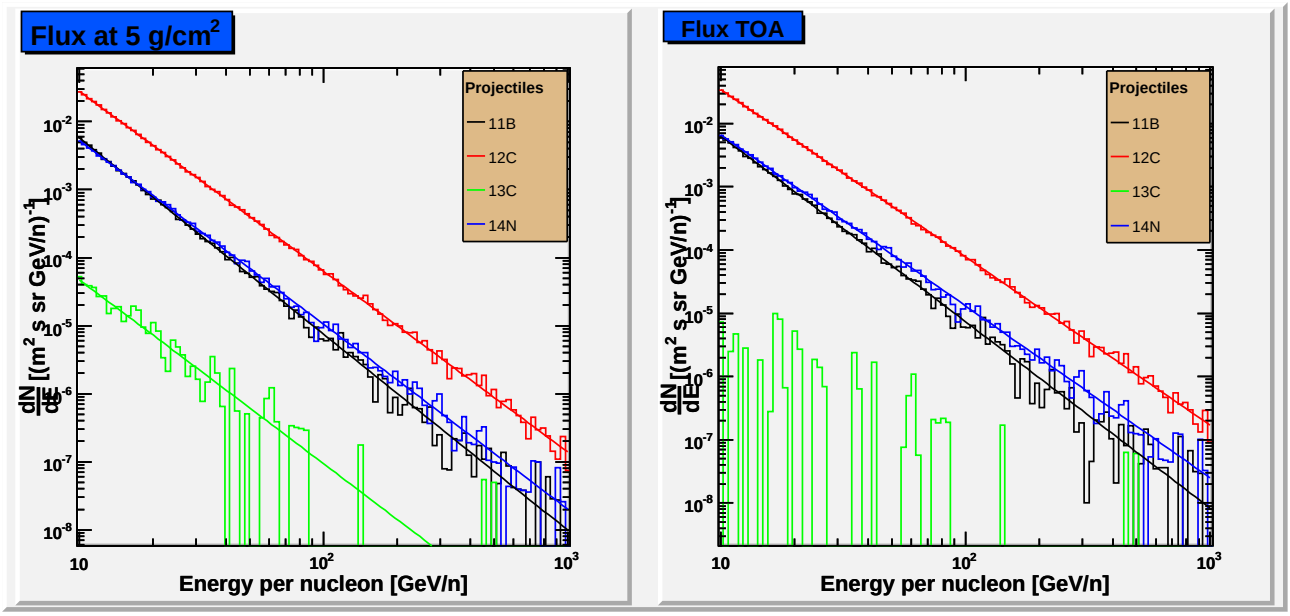

Figure 14: The cosmic ray fluxes at $5\,\mathrm{g/cm^2}$ (solid lines) and the simulation of the detected cosmic-ray spectra at $5\,\mathrm{g/cm^2}$ (histograms) are represented on the left hand side plot. The simulated TOA fluxes (histograms on the right hand side plot) are extracted by inverting the transformation matrix R for testing, if we have an unfolding problem, by comparing to the original cosmic-ray TOA fluxes (solid lines on the right hand side plot).

4.3 Error study

The question, which we want to answer in this section, is, if we have to take into account or not the accuracy at which the used cross sections are currently known. In other words we want to evaluate the systematic errors due to the uncertainties of the cross sections used. This systematical error can be estimated by using a matrix with errors of the cross sections for the inversion and so for the extraction of the cosmic ray TOA fluxes.

In the section 3.1.3 we have seen, that an accuracy of 5% on the total inelastic cross sections is given by the authors. The accuracy of the fragmentation cross section varies between 5% for the reactions with a small $\Delta Z = Z_P - Z_F$ and 10% for the reactions with a high ΔZ. Additionally we have an error on the scaling factor γ_S, which we can not estimate. Consequently, an error of 5% for the total and 10% for the fragmentation cross sections are chosen.

To illustrate this systematic error study, we have chosen to study the influence of the cross sections uncertainties on the estimation of the spectral index δ with the help of the B/C ratio. For this study we only used three different δ, i. e. $\delta = 0.3$, 0.6 and 0.85, obtained from F. Donato [33], for reasons of readability.

The procedure is the follows for each energy E_k:

1. The first step was the extraction from the three different B/C ratios of the ^{11}B and ^{12}C fluxes for the various δ. Then one response matrix $R(x)$, with no additional error on the cross sections, was created. Both the matrix and the fluxes were used for the calculation of the atmospheric fluxes for a given grammage $x\,\mathrm{g/cm^2}$ of atmosphere:
$$\tilde{N}_{\delta_i}(x) = R(x)\tilde{N}_{\delta_i}(0), \tag{56}$$
for the three spectral indices.

2. 100 response matrices with errors on the cross sections $R^{\mathrm{err}}(x)$ were created for each energy E_k. Here an random error of $\pm 5\%$ for each total inelastic cross section and $\pm 10\%$ for each fragmentation cross section was added. With these matrices the atmospheric fluxes at $x\,\mathrm{g/cm^2}$ were calculated for each δ:
$$\tilde{N}^{\mathrm{err}}_{\delta_i}(x) = R^{\mathrm{err}}(x)\tilde{N}_{\delta_i}(0). \tag{57}$$

3. Now for each of the 100 reconstructed TOA fluxes, obtained with the formula
$$\tilde{N}^{\mathrm{err}}_{\delta_i}(0) = R^{-1}(x)\tilde{N}^{\mathrm{err}}_{\delta_i}(x), \tag{58}$$

where the original response matrix $R(x)$ was used, the B/C ratio at each energy E_k was calculated and the minimum and maximum B/C ratios were searched. The six vectors, giving the three minimum and the three maximum B/C ratios, were kept for reconstructing the extremal cosmic ray TOA fluxes.

4. These extremal TOA fluxes permit us to calculate the extremal B/C ratios, by extracting the abundances of the ^{11}B and ^{12}C cosmic-ray nuclei. These are the upper and lower limit of the estimated systematic error for the B/C ratios. The three different zones for the various δ, representing the systematic error area, are shown on figure 15.

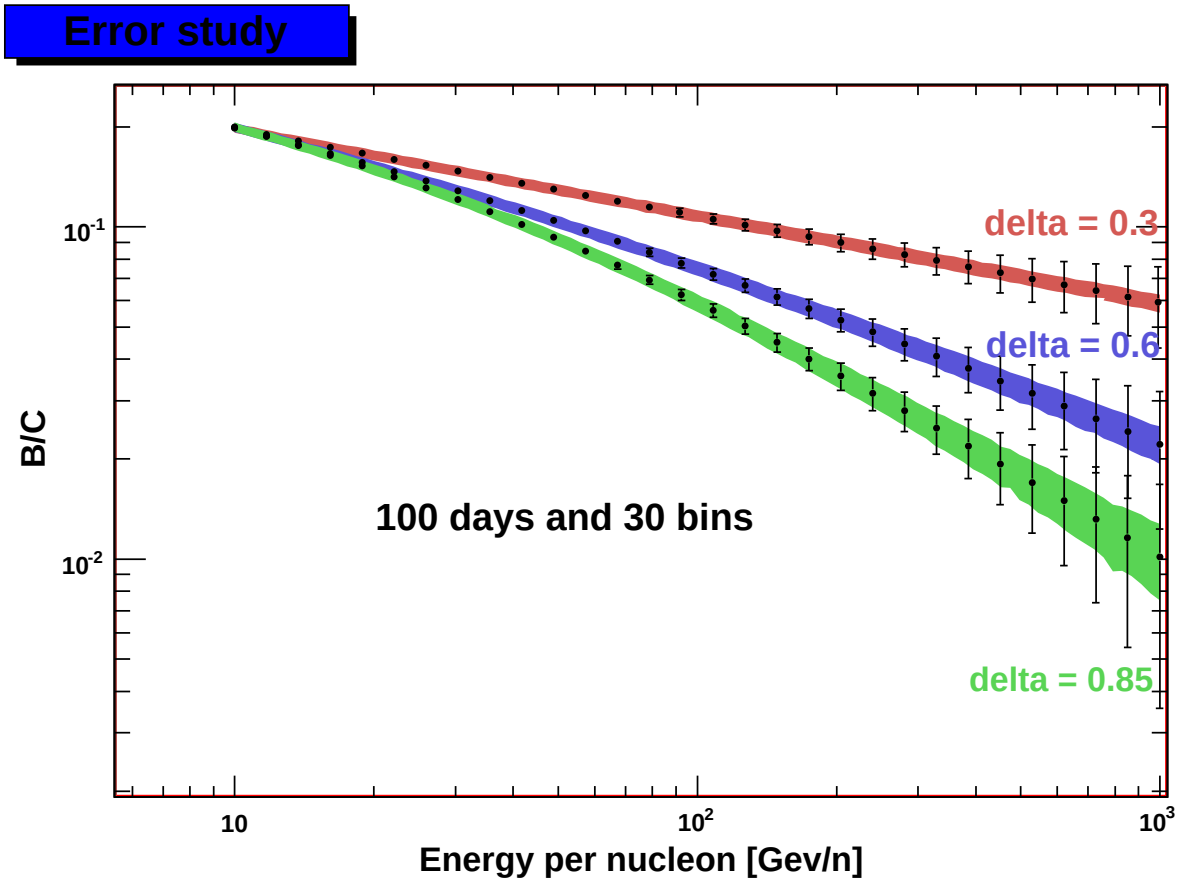

Figure 15: The colored areas represents the systematical error zones for different values of $\delta = 0.3, 0.6, 0.85$. The statistical error is calculated for 100 days and 30 energy bins.

We can see that for $\delta = 0.3$ the systematic error stays small for the whole energy range, in contrary to the $\delta = 0.85$ case, where it becomes more important for increasing energy. This could be explained by the fact, that for the case with $\delta = 0.85$ more secondaries are produced in the Earth's atmosphere proportionally to the secondary galactic population as for the case with a $\delta = 0.3$ (see figure 13(b)). Hence the error on the fragmentation cross sections induces a larger systematic error for a $\delta = 0.85$ as for a $\delta = 0.3$. The great measurement errors, of which the fragmentation cross sections are affected, play a significant role at high energies.

To obtain the value of the systematic error, we have calculated the mean spectral index $\bar{\delta}$ of the extremal B/C ratios over the whole energy range, by interpolating with the three δ values 0.3, 0.6, 0.85 for each energy E_k. We got the following values:

δ	$\bar{\delta}_{\min}$	$\bar{\delta}_{\max}$
0.3	0.29 ± 0.02	0.32 ± 0.03
0.6	0.54 ± 0.02	0.67 ± 0.02
0.85	0.78 ± 0.03	0.93 ± 0.03

So we got the estimated values for the systematic error on the spectral index fitting:

$$\begin{aligned} \delta &= 0.3 \pm 0.02 \\ \delta &= 0.6 \pm 0.07 \\ \delta &= 0.85 \pm 0.08 \end{aligned}$$

For large δ the measurement errors on the cross sections do not allow us to make a clean separation between a $\delta = 0.8$ and $\delta = 0.9$. In contrary for smaller values of δ, here we can distinguish $\delta = 0.3$ and $\delta = 0.35$. The diffusive reacceleration model predicts a delta between 0.5 and 0.75. For these values an incertitude of 0.07 is calculated.

The next question, which we want to answer here, is, what is the statistic needed for the measurements to be dominated by the systematics errors. To respond to this question we assumed that the acceptance A of the detector is $1\,\mathrm{m}^2\,\mathrm{sr}$, the number of energy bins is 30 and the measure time T is equal to 100 days. The corresponding statistical error, given by the formula:

$$\sigma_{\delta_i}^{\mathrm{B/C}} = \sqrt{\frac{N_{B,\delta_i}(0) + N_{C,\delta_i}(0)}{N_{B,\delta_i}(0) \cdot N_{C,\delta_i}(0) \cdot AT\Delta E_k}} N_{B/C,\delta_i}(0) \tag{59}$$

is represented by the error bars on the B/C ratios for the three different spectral indices δ. We can see, that the statistical error is dominant for high energies ($E_k > 200\,\mathrm{GeV/n}$) for the given detector acceptance and measure time, which has been realistically chosen. But a more quantitative study comparable to the study discussed in the paper of A. Castellina and F. Donato (see ref. [33]) have to be made. In order to evaluate the accuracy in the determination of δ due to the statistical errors, the authors performed a χ^2 minimisation procedure on the simulated B/C data, leaving all parameters of the propagation model free. They estimated a statistical uncertainty of about 10-15% on the determination of δ for experiments like CREAM.

4.4 Results

The used matrix method was successfully implemented by using some classes of the USINE software and the ROOT library "TMatrix". This method proved to be easily to handle for the further studies. First, we studied the propagation of some cosmic ray TOA fluxes in the Earth's atmosphere for a grammage of $5\,\mathrm{g/cm}^2$, because this value corresponds the traversed matter of the Earth's atmosphere at an altitude of abount 40 km, which is approximately the altitude in which balloon based experiments like CREAM fly. The overall statement is that the production of secondary particles in the Earth's atmosphere becomes more important for increasing energy, what means that a correction on the measured data becomes necessarily at high energies.

In a second step the propagation of the B/C ratios for different spectral indices δ in the Earth's atmosphere was studied. In comparison to the TOA B/C ratios, the atmospheric B/C ratios flatten at higher energies until they become practically constant. This could be explained by a greater secondary particle production during the traverse of the Earth's atmosphere. The hight energy cosmic ray particles travel through more matter thickness in the atmosphere than in the interstellar medium. The difference of magnitude between the TOA and atmospheric B/C ratio is not negligible and has to be corrected during the data analysis. The case of the B/C ratio for a spectral index $\delta = 0.85$ is more affected as the smaller indices, caused by the larger difference between the interstellar and atmospheric secondary production.

The identification of the spectral index value is a crucial point in astroparticle physics. The measurement of the spectral index by an balloon experiment like CREAM which detects cosmic-ray particles, especially secondary-to-primary ratios, after they have travelled through a given thickness of the Earth's atmosphere, is complicated and effected by some measurement errors, we have to take into account. A response matrix for simulating the expected atmospheric fluxes can be easily inverted for extracting the expectation values of the TOA fluxes from the collected data. But the fact that the experimental data is affected by statistical fluctuations may cause large standard deviations on the reconstructed flux. This is due to the response matrix, which smears out any fine structure of the fluctuation. The unsmearing of the reconstructed data is called unfolding. We have tested successfully that the inversion of the response matrix does not cause any unfolding problem.

It is easier to realise experiments for measuring total inelastic cross sections of nucleus-nucleus reactions as experiments which measure the fragmentation cross sections. So it is comprehensible that these fragmentation cross sections are more affected by measurement errors. But additionally, it is still not realisable to measure all the fragmentation cross sections of nucleus-nucleus reactions. Even if a great number of these cross sections was measured, it is necessary to calculate via different formulations all possible cross sections. We used the formula

of Webber & al, which seems to be the most precise of all the available software, calculating the fragmentation cross sections and the universal parametrisation of Tripathi & al for the total inelastic cross sections. The accuracy of the cross sections used influences the reconstruction of the TOA fluxes from the measured ones. The induced systematical error does not allow to extrapolate an exact value of the spectral index from the reconstructed data, but it permits us to give an upper and a lower limit of it. Additionally, the statistical error induced by the number of detected particles during the measuring time for a given detector dominates this systematical error for high energies. That means that the systematical error is negligible for these energies, which are interesting for the spectral index measurement.

5 Conclusions

After the discovery of the cosmic rays by Viktor Hess in 1912, this phenomenon is still today one of the greatest mysteries of astrophysics. Even if the composition is well known for energies below some TeV and the energy distribution is well observed until an energy of around 10^{18} eV, the sources and the propagation of these ionised particles are yet not known and understood. During the last century a lot of models, which try to explain the observed properties, are conceived, of which the leaky box model is the most successful.

Knowing the abundances of the various kinds of secondary nuclei, produced via spallation while propagating through the interstellar medium, we can determine several parameters of the propagation models of cosmic rays in the Galaxy. This determination allows us to restrict some of these propagation models. Especially the boron-to-carbon ratio has always been considered the best quantity to study diffusion properties. In the leaky box model the relative abundance of stable secondary nuclei is completely determined by the average matter thickness (grammage) traversed by the particles. Additionally this model describes the energy dependence of the traversed matter, explaining the observed B/C ratio, by using a slope, named the spectral index. The spectral index shapes the B/C ratio at high energies and its measurement has become a crucial astrophysical feature, because of its importance for the propagation model constraints.

The direct detection of high energy cosmic rays up to $\sim 10^{15}$ eV could be assured by space based experiments like AMS ($\sim 10^{12}$ eV) or balloon experiments like CREAM. At an energy of 10^{12} eV the B/C ratios differ in approximately one order of magnitude for a spectral index value of 0.3 and 0.85, which permits an easier identification of the exact value from the measured data. For balloon experiments, which fly at an altitude of about 40 km, the direct detection of the cosmic-ray particles is biased by the secondary particles, produced via interaction with atmospheric particles in the Earth's upper atmosphere. For increasing energies this secondary production becomes more important and influences the B/C ratios, measured at a depth of $5\,\mathrm{g/cm^2}$. These become at this depth flatter and practically constant for high energies, where a spectral index of 0.85 is more affected as the smaller indices.

For taking into account the absorption and the secondary production, during the propagation of the cosmic rays in the Earth's atmosphere, a matrix method, estimating this effect, was conceived and implemented. For calculating this response matrix the total and partial inelastic cross sections of nucleus-nucleus reactions were needed. Some approaches exist to calculate these cross sections, which have been presented in this thesis and two of them were used for the matrix calculation. Here we got help from David Maurin, who provides his USINE software for the implementation. The matrix method is easy to handle and permits the reconstruction of the top of atmosphere fluxes from the measured atmospheric fluxes. For this reconstruction the matrix had to be inverted, which could cause unfolding problems. The procedure of correcting distortions, due to statistical errors, is known as unfolding. In this work, we tested our response matrix for unfolding problems for a atmospheric depth of $5\,\mathrm{g/cm^2}$, a measuring time of 100 days, a detector acceptance of $1\,\mathrm{m^2\,sr}$, and 30 energy bins for the whole considered energy range. Because the eigenvalues of the corresponding response matrix are close to one, no unfolding problem had been observed and therefore, there is no need to unfold the reconstructed data for this depth.

By using the calculated cross sections, we have to be aware of the introduced systematic errors in our reconstruction, induced by the errors on the cross sections. The influence of the systematic errors on the B/C ratios had been analysed for three different spectral indices. Large spectral indices are more affected at high energies by the systematical error as smaller indices. This systematical error was calculated by using an error of 10% on the fragmentation cross sections and 5% on the total inelastic cross sections. This does not allow us to make an exact extrapolation of the spectral index from the data taken, but we can estimate lower and upper limits for it, which had been calculated for three different spectral indices. At last, the statistical error of the data had been analysed. For all the spectral indices examined the statistical error dominates the systematical error up to an energy of around 200 GeV/n for a measuring time of 100 days a detector acceptance of $1\,\mathrm{m^2\,sr}$, and 30 energy bins for the whole considered energy range.

The propagation of cosmic rays in the Earth's atmosphere and its effects on data have been investigated. A method for an extrapolation to the TOA fluxes has been conceived, successfully implemented, and tested. The influence of the errors on the cross sections has been estimated for various spectral indices. This conceived method can be easily enlarged to calculate the interaction of cosmic rays in the detectors itself. For this additionally, a simulation of the detectors AMS and CREAM would permit the preparation of the data analysis for these two detectors. In this thesis only perpendicular fluxes were considered. A next step would be to take into account the zenith angle, under which the cosmic rays arrive on the detector. In order to generate a general program, applicable to other detectors, additionally features will be implemented.

Bibliography

Astrophysics of Cosmic Rays

[1] V. S. Berenzinskii & al.; *Astrophysics of cosmic rays* (North-Holland, 1990).

[2] Malcolm S. Longair; *High Energy Astrophysics*; vol. 1 Particles, photons and their detection (Cambridge University Press, 1992).

A little bit of history...

[3] Georg Federmann; *Viktor Hess und die Entdeckung der Kosmischen Strahlung*; Master's thesis; Institut für Radiumforschung und Kernphysik, Wien, **2003**.

General cosmic ray properties

[4] Swordy, S.; *Cosmic Ray Spectrum Picture*; University of Chicago; http://astroparticle.uchicago.edu/cosmic_ray_spectrum_picture.htm.

[5] T. K. Gaisser & T. Stanev; astro-ph/0510321 .

[6] David Maurin; *Propagation des rayons cosmiques dans un modele de diffusion: une nouvelle estimation des paramètres de diffusion et du flux d antiprotons secondaires*; Ph.D. thesis; Université de Savoie, **2001**.

[7] I. Lerche and R. Schlickeiser; A&A 151:(1985), 408–420.

[8] Bruny Baret; *Simulation et détection du Rayonnement Cosmique: Production d'antimatière dans l'atmosphère et étude de l'imageur Cherenkov annulaire de l'expérience AMS*; Ph.D. thesis; Université Joseph Fourier - Grenoble I, **2004**.

[9] F. C. Jones, A. Lukasiak, V. Ptuskin and W. Webber; astro-ph/0007293 .

Solar modulation and TOA fluxes

[10] E. N. Parker; ApJ 128:(1958), 664.

[11] L. J. Gleeson and W. I. Axford; ApJ 154:(1968), 1011.

[12] M. L. Duldig; astro-ph/0010147 .

[13] Feimer, W.; *Voyager Enters Solar System's Final Frontier*; NASA, **2005**; http://www.nasa.gov/vision/universe/solarsystem/voyager_agu.html.

[14] Barbara Wiebel-Sooth, Peter L. Biermann and Hinrich Meyer; Astron. Astrophys. 330:(1998), 389–398.

Detection of cosmic rays

[15] *Astroteilchenphysik in Deutschland*; http://www.astroteilchenphysik.de.

[16] NASA; *Balloon Program Office*; http://www.wff.nasa.gov/~ code820/.

[17] LPSC Grenoble; *AMS Grenoble Homepage*; http://lpsc.in2p3.fr/ams/ams-eng/general.html.

[18] University of Maryland; *CREAM Home*; http://cosmicray.umd.edu/cream/cream.html.

[19] Forschungszentrum Karlsruhe; *Homepage of KASCADE-Grande*; http://www-ik.fzk.de/KASCADE/.

[20] *Pierre Auger Observatory*; http://www.auger.org/index.html.

Earth's atmosphere

[21] National Oceanic and Atmospheric Administration (NOAA); *Jetstream*; http://www.srh.noaa.gov/srh/jetstream/atmos/layers.htm.

[22] A. E. Hedin; Journal of Geophysical Research 96(A2):(1991), 1159–1172.

Total inelastic cross sections

[23] W. R. Webber, J. C. Kish and D. A. Schrier; Phys. Rev. C 41(2):(1990), 520.

[24] J. R. Letaw, R. Silberberg and C. H. Tsao; ApJSS 51:(1983), 271–276.

[25] R. K. Tripathi, F. A. Cucinotta and J. W. Wilson; NASA Technical Paper 3621.

[26] R. K. Tripathi, F. A. Cucinotta and J. W. Wilson; NASA Technical Paper 209726.

Fragmentation cross sections

[27] R. Silberberg and C. H. Tsao; ApJSS 25:(1973), 315–333.

[28] L. Sihver, C. H. Tsao, R. Silberberg, T. Kanai and A. F. Barghouty; Phys. Rev. C 47(3):(1993), 1225.

[29] W. R. Webber, J. C. Kish and D. A. Schrier; Phys. Rev. C 41(2):(1990), 566.

[30] P. Ferrando, W. R. Webber, P. Goret, J. C. Kish, D. A. Schrier, A. Soutoul and O. Testard; Phys. Rev. C 37(4):(1988), 1490.

[31] D. L. Olson, B. L. Berman, D. E. Greiner, H. H. Heckman, P. J. Lindstrom and H. J. Crawford; Phys. Rev. C 28(4):(1983), 1602.

USINE software

[32] Maurin, D.; *Private communication*.

Study of the fragmentation process in the Earth's atmosphere

[33] A. Castellina and F. Donato; Astropart. Phys. 24:(2005), 146–159.

[34] Cowan, G.; *Statistical Data Analysis* (Oxford Science Publications, 1998).